

# 3D Gaussian Splatting: Survey, Technologies, Challenges, and Opportunities

Yanqi Bao, Tianyu Ding, Jing Huo, Yaoli Liu, Yuxin Li, Wenbin Li, and Yang Gao, *Member, IEEE*,  
Jiebo Luo, *Fellow, IEEE*,

**Abstract**—3D Gaussian Splatting (3DGS) has emerged as a prominent technique with the potential to become a mainstream method for 3D representations. It can effectively transform multi-view images into explicit 3D Gaussian representations through efficient training, and achieve real-time rendering of novel views. This survey aims to analyze existing 3DGS-related works from multiple intersecting perspectives, including related tasks, technologies, challenges, and opportunities. The primary objective is to provide newcomers with a rapid understanding of the field and to assist researchers in methodically organizing existing technologies and challenges. Specifically, we delve into the optimization, application, and extension of 3DGS, categorizing them based on their focuses or motivations. Additionally, we summarize and classify nine types of technical modules and corresponding improvements identified in existing works. Based on these analyses, we further examine the common challenges and technologies across various tasks, proposing potential research opportunities.

**Index Terms**—3D Gaussian Splatting, Rendering, Technologies.

arXiv:2407.17418v1 [cs.CV] 24 Jul 2024

## 1 INTRODUCTION

THE advent of Neural Radiance Fields (NeRF) has ignited considerable interest in the pursuit of photorealistic 3D content. Despite substantial recent advancements that have markedly enhanced NeRF’s potential for practical applications, its inherent efficiency challenges have remained unresolved. The introduction of 3D Gaussian Splatting (3DGS) has decisively addressed this bottleneck, enabling high-quality real-time ( $\geq 30$  fps) novel view synthesis at 1080p resolution. This rapid development has quickly garnered significant attention from researchers and has led to a proliferation of related works.

Owing to the efficiency and controllable explicit representation of 3DGS, its applications extend across a diverse array of fields. These include enhancing immersive environments in Virtual Reality (VR) and Augmented Reality (AR), improved spatial awareness in robotics and autonomous systems, advanced visual effects in film and animation, and urban planning and architecture, etc.

To assist readers in quickly grasping the progress in 3DGS research, we provide a comprehensive survey of 3DGS and its downstream tasks. This survey systematically compiles the most important and recent literature on the subject, offering detailed classifications and discussions of their focuses and motivations. However, we find that a considerable number of similar techniques are inevitably mentioned across different tasks. Therefore, we further summarize and classify the various technical modules of 3DGS, such as initialization, attribute setting, and regularization, etc. Based on this

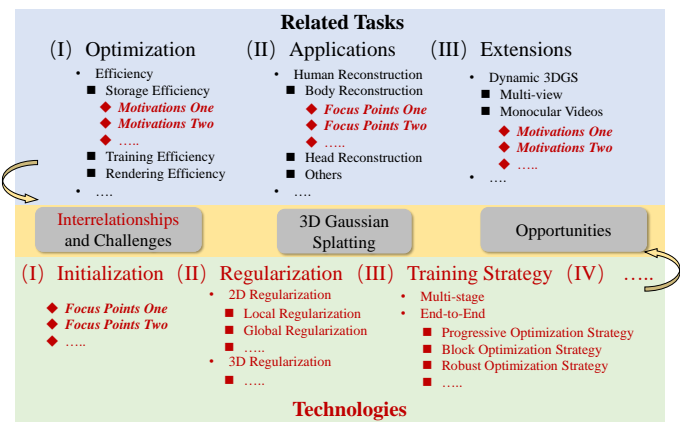


Fig. 1: The introduction of this survey, with the parts marked in RED indicating the new content compared to existing reviews.

summary of techniques, we aim to help readers elucidate the connections between different technologies and enhance various components of 3DGS to meet their customized tasks. Additionally, we investigate the interrelationships between various downstream tasks and technologies in 3DGS, systematically delineating four principal challenges to facilitate future research in this domain. Finally, we emphasize the limitations of existing research and propose promising avenues to address core challenges and advance this rapidly evolving field.

Although several studies have summarized the recent advances in 3DGS [1], [2], [3], our goal is to **systematically discuss and fine-grainedly classify** the related tasks and **techniques** of 3DGS, and analyze the **commonalities** and challenges between them, as illustrated in Fig. 1. Specifically, the main contributions of this survey are as follows:

- 1) This survey discusses 3DGS and its various derivative

- Yanqi Bao, Jing Huo, Yaoli Liu, Yuxin Li, Wenbin Li and Yang Gao are with the State Key Laboratory for Novel Software Technology, Nanjing University, China, 210023 (e-mail: {yq\_bao, yaoliliu, liyuxin16}@smail.nju.edu.cn; {huojing, liwenbin, gaoy}@nju.edu.cn).
- Tianyu Ding is with the Applied Sciences Group, Microsoft Corporation, Redmond, USA (e-mail: tianyuding@microsoft.com).
- Jiebo Luo is with the Department of Computer Science, University of Rochester, America (e-mail: jluo@cs.rochester.edu).
- \*Corresponding authors: Jing Huo.

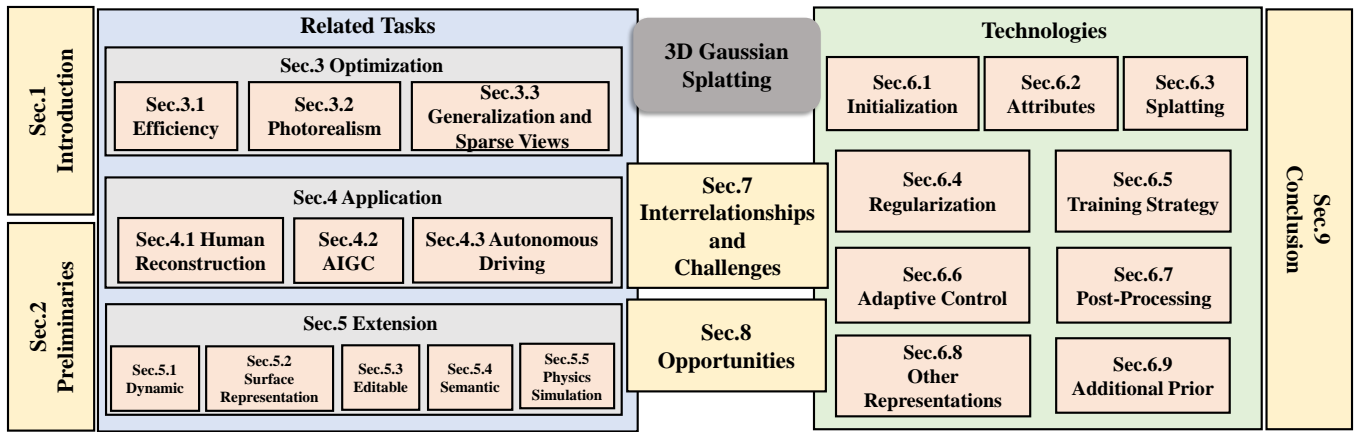


Fig. 2: Structure of this Survey, including Related Tasks, Technologies, Challenges, and Opportunities.

tasks, including the optimization, application, and extension of 3DGS. Unlike existing reviews, we provide a more detailed classification based on *focuses or motivations*, which enables readers to gain a more comprehensive understanding of tasks and establish research directions.

- 2) More importantly, we comprehensively analyze the enhancements in various techniques within 3DGS as presented in existing literature, offering detailed classifications and in-depth discussions. This enables readers to discern the commonalities among various improved techniques, thereby assisting in their application to customized tasks.
- 3) Based on the analysis of existing works and techniques, we identify the commonalities and associations among 3DGS-related tasks and summarize the core challenges.
- 4) In addressing common challenges, this survey elucidates potential opportunities and provides insightful analyses.
- 5) We have published an open-source project on GitHub that compiles 3DGS-related articles, and will continue to add new works and technologies into this project. <https://github.com/qqqqqy0227/awesome-3DGS>. We hope that more researchers can use it to access the latest research information.

As depicted in Fig.2, the structure of this survey is organized as follows: Sec.2 describes the background and details of 3D Gaussian Splatting (3DGS), emphasizing its advantages over Neural Implicit Fields and Point-based Rendering. Sec.3 focuses on optimizing 3DGS to address challenges encountered during the reconstruction process. Sec.4 summarizes the applications of 3DGS and discusses its implementation in downstream tasks. Sec.5 provides an overview of the extensions of 3DGS, exploring ways to enhance its original capabilities. Sec.6 consolidates the various techniques for improving 3DGS modules. Sec.7 reviews the interrelationships among different tasks as well as technologies and summarizes core challenges. Finally, Sec.8 outlines promising avenues for future research, addressing existing challenges and technical optimizations and Sec.9 summarizes this survey.

It should be noted that this survey does not provide an

overview of datasets; detailed information can be found in previous reviews [3], [4]. Additionally, in the first half of the article, we primarily describe how existing works address the downstream tasks of 3DGS, while the second half focuses on technologies. Although some repeated works are mentioned, the points of focus and content differ.

## 2 PRELIMINARIES

### 2.1 Neural Implicit Field

Neural implicit field representations have garnered significant attention in recent research [5], [6]. These methodologies conceptualize 2D or 3D signals to be reconstructed as fields within corresponding Euclidean spaces, utilizing discrete samples to train neural networks that approximate these fields. This approach facilitates the reconstruction, interpolation, and extrapolation of the original discrete samples, enabling applications such as the super-resolution of 2D images and novel view synthesis of 3D scenes. In the specific context of 3D reconstruction and novel view synthesis, Neural Radiance Fields (NeRF) [7] leverage neural networks to model the geometry and appearance of 3D scenes as density fields and radiance fields. NeRF employs volumetric rendering to establish a mapping from the 3D field to 2D images, thus enabling the reconstruction of 3D signals from multiple 2D images and facilitating novel view rendering. Among the current state-of-the-art methods in this domain, Mip-NeRF 360 [8] stands out for achieving superior rendering quality, while Instant-NGP [9] is notable for its exceptional training efficiency.

However, neural implicit field methods heavily rely on the volumetric rendering process to obtain rendered pixels. This process requires sampling tens to hundreds of points along each ray and inputting them into the neural network to produce the final imaging result. Consequently, rendering a single 1080p image necessitates on the order of  $10^8$  neural network forward passes, which often takes several seconds. Although some works employ explicit, discretized structures to store continuous 3D fields, thereby minimizing the dependency on neural networks and accelerating the query process for field representations [9], [10], [11], the vast

number of sampling points still incurs extremely high rendering costs. Such methods based on volumetric rendering incapable of achieving real-time rendering, thereby limiting their applicability in downstream tasks.

## 2.2 Point-based Rendering

Since continuous 3D fields do not distinguish between occupied and unoccupied spaces within a scene, a significant number of sampling points during the volumetric rendering process are located in unoccupied spaces. These sampling points contribute minimally to the final rendering result, leading to low rendering efficiency. In contrast, discrete point cloud representations only record the truly occupied parts of the 3D scene, offering a more efficient and precise way to represent the scene. Rendering based on point clouds relies on rasterization rather than stochastic sampling, allowing the use of modern GPUs for real-time rendering.

However, existing high-quality differentiable rendering methods based on point clouds typically depend on pre-constructed point clouds or require dense point cloud reconstruction. These methods do not further optimize the point cloud structure during training [12], [13], [14], resulting in rendering quality that is highly dependent on the initial point cloud quality and making the final images prone to artifacts or incorrect appearances.

## 2.3 3D Gaussian Splatting

3D Gaussian Splatting [15] combines the advantages of neural implicit field and point-based rendering methods, achieving the high-fidelity rendering quality of the former while maintaining the real-time rendering capability of the latter, as shown in Fig. 3. Specifically, 3DGS defines points in the point cloud as 3D Gaussian primitives with volumetric density:

$$G(\mathbf{x}) = \exp\left(-\frac{1}{2}(\mathbf{x})^T \Sigma^{-1}(\mathbf{x})\right), \quad (1)$$

where  $\Sigma$  is the 3D covariance matrix and  $\mathbf{x}$  is the position from the point (Gaussian mean)  $\boldsymbol{\mu}$ . To ensure the semi-positive definiteness of the covariance matrix, 3DGS reparameterizes the covariance matrix as a combination of a rotation matrix  $\mathbf{R}$  and a scaling matrix  $\mathbf{S}$ :

$$\Sigma = \mathbf{R}\mathbf{S}\mathbf{S}^T\mathbf{R}^T, \quad (2)$$

where the 3D scaling matrix  $\mathbf{S}$  can be represented by a 3D vector  $\mathbf{s}$ , and the rotation matrix  $\mathbf{R}$  is obtained through a learnable quaternion  $\mathbf{q}$ , resulting in a total of 7 learnable parameters. Compared to the commonly employed Cholesky decomposition, which guarantees the semi-positive-definiteness of matrices, the reparameterization method utilized by 3DGS, albeit introducing an additional learnable parameter, facilitates the imposition of geometric constraints on Gaussian primitives (e.g., constraining the scaling vector to give Gaussian primitives a flattened characteristic). In addition to geometric attributes, each Gaussian primitive also stores an opacity  $\alpha$  and a set of learnable Spherical Harmonic (SH) parameters to represent view-dependent appearance. Thus, the collection of all primitives

can be regarded as a discretized representation that only stores the non-empty parts of the neural field.

During rendering, 3DGS projects 3D Gaussian primitives onto the 2D imaging plane using the EWA splatting method [16] and employs  $\alpha$  blending to compute the final pixel color. This rendering process, for each pixel, is analogous to the discrete form of volumetric rendering used in neural fields, enabling 3DGS to construct complex scene appearances and achieve high-quality rendering. To achieve high-frame-rate, high-resolution differentiable rendering, 3DGS utilizes a tile-based rasterizer. This rasterizer first divides the image into  $16 \times 16$  tiles and assigns an index to each tile. For each Gaussian primitive, the rasterizer determines which tiles the primitive's projection intersects and generates a key-value pair for each intersecting tile: the key is 64-bit, with the upper 32 bits representing the tile index and the lower 32 bits representing the projection depth of the Gaussian primitive. By constructing these key-value pairs, the rasterizer only needs to perform a global sort on all key-value pairs, eliminating the need for additional sorting of primitives for each pixel. After sorting, the key-value pairs derived from each tile reside in contiguous memory intervals. The rendering process for each tile is then managed by a CUDA thread block, with the number of threads within each block matching the number of pixels in the tile. Each thread is responsible for the  $\alpha$  blending process for its corresponding pixel, thus completing the final rendering.

At the beginning of training, the initial Gaussian primitives are either initialized from a sparse point cloud provided by Structure-from-Motion or randomly initialized. The initial number of Gaussian primitives may be insufficient for high-quality scene reconstruction; hence, 3DGS offers a method for adaptively controlling Gaussian primitives. This method evaluates whether a primitive is "under-reconstructed" or "over-reconstructed" by observing the gradient of each Gaussian primitive's position attributes in view space. Based on this evaluation, the method increases the number of Gaussian primitives by cloning or splitting the primitives to enhance scene representation capability. Additionally, the opacity of all Gaussian primitives is periodically reset to zero to mitigate the presence of artifacts during the optimization process. This adaptive process allows 3DGS to start optimization with a smaller initial set of Gaussians, thus alleviating the dependency on dense point clouds that previous point-based differentiable rendering methods required.

## 3 OPTIMIZATION OF 3D GAUSSIAN SPLATTING

### 3.1 Efficiency

Efficiency is one of the core metrics for evaluating 3D reconstruction. In this section, we describe it from three perspectives: storage, training, and rendering efficiency.

#### 3.1.1 Storage Efficiency

3DGS requires millions of different Gaussian primitives to fit the geometry and appearance in a scene, leading to high storage overhead: a typical reconstruction of an outdoor scene often requires several hundred megabytes to multiple gigabytes of explicit storage space. Given that the geometric and appearance attributes of different Gaussian primitives

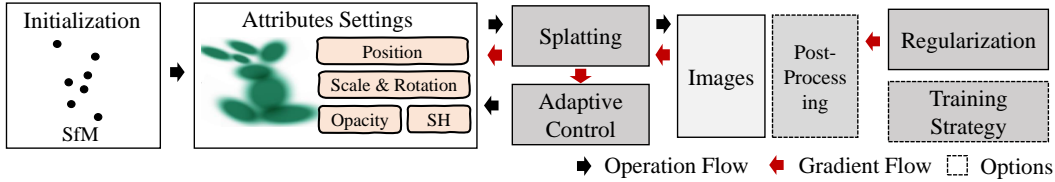


Fig. 3: Pipeline and Related Technologies of 3D Gaussian Splatting.

may be highly similar, storing attributes for each primitive individually can lead to potential redundancy.

Therefore, existing works [17], [18], [19] primarily focus on applying Vector Quantization [20] (VQ) techniques to compress large numbers of Gaussian primitives.

Compact3D [18] applies VQ to compress different attributes into four corresponding codebooks and stores the index of each Gaussian in these codebooks to reduce the storage overhead. After establishing the codebooks, the training gradients are copied and backpropagated to the original non-quantized Gaussian parameters via the codebooks, updating both the quantized and non-quantized parameters, and discarding the non-quantized parameters when the training is done. Additionally, Compact3D employs run-length coding to compress the sorted index values further, thereby enhancing storage efficiency. Similarly, the work by Niedermayr et al. [19] proposes a sensitivity-aware vector quantization technique to construct codebooks based on sensitivity-aware k-means [21] and utilizes the DEFLATE compression algorithm [22] to further compress the trained codebooks. After training, it proposes a quantization-aware fine-tuning strategy to recover information lost due to VQ.

Furthermore, some works [23], [24], [25] aim at developing pruning strategies or compressing SH parameters.

Some works [23], [24] consider both simultaneously. LightGaussian [24] introduces a Gaussian pruning strategy based on the global significance score and a distillation strategy for high-degree spherical harmonic parameters. Similarly, the work by Lee et al. [23] introduces a learnable mask to reduce the number of original Gaussians and a unified hash-grid-based appearance field [9] to compress the color parameters.

Unlike the aforementioned works, Self-Organizing Gaussian [25] does not use traditional nontopological VQ codebooks for compressing large numbers of Gaussians. Instead, it employs the concept of self-organizing mapping to map Gaussian attributes into corresponding 2D grids. The topological relationships in the 2D grids reflect those in the original attribute space, allowing compression algorithms for topologically structured 2D data to be applied to the unordered Gaussian primitives.

Additionally, there are works [26], [27] focused on improving efficient Gaussian representations.

Scaffold-GS [26] designs anchors and additional attributes for efficient representation, which have the capability to convert to 3DGS. Based on this representation, Scaffold-GS proposes a set of strategies for the growth and pruning of anchors on multi-resolution voxel grids.

GES [27] introduces the Generalized Exponential (GEF) Mixture to replace Gaussian representations, which has the capability to efficiently fit arbitrary signals. By designing

a Fast Differentiable Rasterizer and Frequency-Modulated Image Loss for GEF, GES is capable of utilizing a smaller number of GEF primitives while maintaining performance.

### 3.1.2 Training Efficiency

Improving training efficiency is also important for 3DGS. DISTWAR [28] introduces an advanced technique aimed at accelerating atomic operations in raster-based differentiable rendering applications, which typically encounter significant bottlenecks during gradient computation due to the high volume of atomic updates. By leveraging intra-warp locality in atomic updates and addressing the variability in atomic traffic among warps, DISTWAR implements warp-level reduction of threads at the SM sub-cores using registers. Furthermore, it dynamically distributes atomic computations between the SM and L2 atomic units. This software-only implementation employs existing warp-level primitives to minimize the number of atomic operations directed to L2, thereby significantly enhancing throughput.

### 3.1.3 Rendering Efficiency

Real-time rendering is one of the core advantages of Gaussian-based methods. Some works that improve storage efficiency can simultaneously enhance rendering performance, for example, by reducing the number of Gaussian primitives. Here, we discuss additional works contributing to these advancements.

After training the 3DGS, the work by [29] involves pre-identifying and excluding unnecessary Gaussian primitives through offline clustering based on their spatial proximity and potential impact on the final rendered 2D image. Furthermore, this work introduces a specialized hardware architecture designed to support this technique, achieving a speedup of 10.7× compared to a GPU.

GSCore [30] proposes a hardware acceleration unit for optimizing the rendering pipeline of 3DGS in radiance field rendering. Based on the analysis of performance bottlenecks in Gaussian sorting and rasterization, GSCore introduces optimization techniques such as Gaussian shape-aware intersection tests, hierarchical sorting, and subtile skipping. Implementing these techniques within GSCore results in a 15.86× average speedup over mobile GPUs.

## 3.2 Photorealism

Photorealism is also a topic worth attention [31]. 3DGS is expected to achieve realistic rendering in various scenarios. Some [32], [33] focus on *optimizing in its original settings*.

To alleviate the dependence on SfM initialization, GaussianPro [32] introduces an innovative paradigm for joint 2D-3D training. Building upon the 3D plane definition and patch

matching technology, it proposes a progressive Gaussian propagation strategy, which harnesses the consistency of 3D views and projection relationships to refine the rendered 2D depth and normal maps. Following geometric filtering and selection processes, the optimized depth and normal maps are employed for densification and additional supervision, ultimately achieving precise geometric representation.

FreGS [33] transitions the supervision process into the frequency domain and employs amplitude and phase attributes from the 2D discrete Fourier transform to alleviate over-reconstruction in 3DGS. Based on this idea, FreGS introduces a frequency-domain-guided coarse-to-fine annealing technique to eliminate undesirable artifacts.

*The sharp decline in multi-scale rendering performance is also a topic worth attention [34], [35].*

The work [34] first analyzes the causes of aliasing in the frequency domain at low resolutions and in far-away rendering, utilizing Multi-Scale Gaussians to address this issue. Then, Pixel Coverage is defined to reflect the Gaussian size compared to the current pixel size. Based on this concept, it identifies small Gaussians and aggregates them into larger Gaussian for multi-scale training and selective rendering.

Mip-splatting [35], similarly addressing the issue from the perspective of the sampling rate, introduces a Gaussian low-pass filter based on Nyquist’s theorem to constrain the frequency of the 3D Gaussians according to the maximal sampling rate across all observed samples. To address aliasing and dilation artifacts, Mip-splatting replaces the traditional 2D dilation filter with a 2D Mip filter, which approximates a 2D box filter. Unlike modifications in the training phase, SA-GS [36] operates solely by a 2D scale-adaptive filter during test time, making it applicable to any pretrained 3DGS.

*Other works attempt to reconstruct challenging scenes, such as reflective surfaces [37], [38], [39], and Relightable [40].*

GaussianShader [37] reconstructs reflective surfaces by employing a hybrid color representation and integrating the specular GGX [41] and normal estimation module, which encompasses diffuse color, direct specular reflection, and a residual color component that accounts for phenomena such as scattering and indirect light reflections. Also, GaussianShader introduces shading attributes and a normal-geometry consistency constraint in 3DGS during the training process.

Mirror-3DGS [38] adds a learnable mirror attribute to determine the location of mirrors and introduces a Virtual Mirrored Viewpoint to aid in the reconstruction of mirror scenes based on the original 3DGS. And, Spec-Gaussian [39] replaces the original 3DGS with Anisotropic Spherical Gaussian to construct scenes with specular and anisotropic components and introduces an Anchor-based representation [26] for efficiency.

Relightable 3D Gaussian (R3DG) [40] represents 3D scenes using relightable points, each characterized by a normal direction, BRDF parameters, and incident lighting, where the incident lights are decomposed into global and local components with view-dependent visibilities. Then, a novel point-based ray-tracing technique, based on bounding volume hierarchy, is designed in R3DG for efficient visibility baking and real-time rendering with accurate shadow effects.

DeblurGS [42] tackles the challenge of inaccurate camera poses caused by severe blur, which impedes the effectiveness

of Structure-from-Motion (SfM). DeblurGS optimizes sharp 3D scenes by estimating the 6-Degree-of-Freedom (6-DoF) camera motion for each blurry observation and synthesizing corresponding blurry renderings. It also introduces a Gaussian Densification Annealing strategy for training stability.

### 3.3 Generalization and Sparse Views

The challenges of generalization and reconstruction under sparse view settings have long attracted significant scholarly attention. Both implicit representations, such as NeRF, and explicit representations, like 3DGS, face substantial obstacles to practical application due to the necessity of re-training for each scene and the high demand for dense sample inputs. In this section, we discuss their experimental setups and provide a more detailed understanding of existing works.

#### 3.3.1 Generalizable 3D Gaussian Splatting

The objective of existing generalizable 3D reconstruction or novel view synthesis tasks is to leverage extensive auxiliary datasets to learn scene-agnostic representations. In the research on NeRF [43], [44], [45], this process typically involves inputting a small number (1-10) of reference images with adjacent poses to infer the target image. The radiance field functions as an intermediary, effectively obviating the need for explicit scene reconstruction and transforming the task into a scene-agnostic novel view synthesis problem.

In contrast, the 3DGS’s explicit representation has led to a substantial body of works focused on *using reference images to directly infer corresponding Gaussian primitives on a per-pixel basis*, which are subsequently employed to render images from target views.

To achieve this, early works such as Splatter Image [46] propose a novel paradigm for converting images into Gaussian attribute images, thereby predicting the Gaussian primitives corresponding to each pixel. This paradigm is then extended to multiple reference images for better rendering performance.

However, unlike the generalization efforts in NeRF, the training difficulty for generalizable 3DGS increases significantly. Operations such as non-differentiable densification can negatively impact the generalization training process. Addressing these challenges, pixelSplat [47] aims to predict a probabilistic depth distribution from features extracted using an epipolar transformer structure [44] and sample this distribution to replace the non-differentiable components.

Moreover, *methods based on Multi-View Stereo (MVS)* have consistently achieved significant success in scene reconstruction and novel view synthesis, particularly with the introduction of cost volumes, which enhance the network’s spatial understanding. Similar to methods in MVSNeRF [48], MVSplat [49] proposes representing the cost volume using plane sweeps in 3D space and predicting the depths in sparse reference inputs, precisely locating the centers of Gaussian primitives. This approach provides valuable geometric cues for novel view synthesis.

*Additionally, some studies [50], [51] focus on introducing triplane to achieve generalization capabilities.*

The work [50] introduces a point-cloud representation decoder and a triplane representation decoder based on reference features. Through parallel decoding, they construct

a hybrid representation that combines explicit point clouds with implicit triplane fields, enabling the Gaussian Decoder to directly predict Gaussian attributes after position query. Building on similar representations, AGG [51] introduces a pseudo-label-based initialization method and a multi-stage training strategy. This strategy encompasses coarse Gaussian generation followed by super-resolution using reference image features, thereby producing detailed outputs.

### 3.3.2 Sparse Views Setting

Reconstructing from sparse inputs presents significant challenges, wherein the methodology of 3DGS is fundamentally analogous to that of NeRF, *which aim to develop novel regularization strategies and integrate supplementary information, such as depth data.*

Chung et al. [52] propose employing a monocular depth estimation model to predict depth maps, which are subsequently refined using SfM [53] for precise depth range. Additionally, their work incorporates depth smoothness loss and two modified techniques tailored for scenarios with limited samples. Building upon the depth supervision, FSGS [54] introduces a proximity-guided Gaussian upsampling method to increase the quantity and integrates new pseudo-views through a 2D prior model to further mitigate overfitting.

Subsequently, Touch-GS [55] extends this paradigm with tactile sensing in robotic perception applications. After aligning with monocular depth information, tactile sensing data effectively predict corresponding depth and uncertainty maps based on implicit surface representations, which are used to enhance the initialization and optimization processes.

Furthermore, DNGaussian [56] explores the problem from a regularization perspective, proposing two different regularization: hard depth and soft depth, to address the degradation of scene geometry. Then, DNGaussian introduces both global and local depth normalization methods to enhance sensitivity to subtle local depth variations.

*Some studies have focused on the initialization and training strategy.* GaussianObject [57] introduces an initialization strategy based on Visual Hull and an optimization method using distance statistical data to eliminate floaters. Additionally, GaussianObject designs a Gaussian repairing module, which includes data acquisition, training, and inference paradigms, thus leveraging pre-trained models to address occlusions and information loss under sparse viewpoint conditions.

## 4 APPLICATIONS OF 3D GAUSSIAN SPLATTING

3DGS excels in various application domains due to its efficiency and photorealistic renderings, which include digital human reconstruction, Artificial Intelligence Generated Content (AIGC), and autonomous driving, among others. Building on prior explorations, 3DGS can be directly applied as a core technology in diverse research areas, effectively replacing traditional 3D representations.

### 4.1 Human Reconstruction

The application of 3DGS for digital human-related tasks, including human reconstruction, animation, and human generation, has garnered substantial attention within the research community. Recent works can be categorized according to the reconstructed parts.

TABLE 1: Comparison to Works for Body Reconstruction.

	Pose-dependent Deformation	Novel Pose Animation	Fast Training	High Real-time Rendering	Monocular Input	Super-resolution (>60FPS)	Generalization	
✓	✓	✗	✗	✓	✗	✗		HuGS [58]
-	-	-	-	-	✓	✓		GPS-Gaussian [59]
✗	✓	✓	✓	✓	✗	✗		HUGS [60]
✓	✓	✓	✓	✓	✗	✗		GaussianAvatar [61]
✗	✗	✓	✓	✓	✗	✗		GauHuman [62]
✓	✓	✓	✗	✓	✗	✗		3DGS-Avatar [63]
✓	✓	-	✗	✓	✗	✗		ASH [64]
✓	✓	✗	✗	✗	✗	✗		Animatable Gaussian [65]

#### 4.1.1 Body Reconstruction

Body reconstruction mainly focuses on reconstructing deformable human avatars from multi-view or monocular videos, as well as providing real-time rendering. We list comparisons of recent works in Tab. 1.

*Most works [58], [60], [61], [62], [63] prefer to use well-preconstructed human models like SMPL [66] or SMPL-X [67] as strong prior knowledge.* Nevertheless, SMPL is limited to introducing prior knowledge about the human body itself, thus posing challenges for the reconstruction and deformation of outward features such as garments and hair.

*For the reconstruction of outward appearance,* HUGS [60] utilizes SMPL and LBS only at the initial stage, allowing Gaussian primitives to deviate from the initial mesh to accurately represent garments and hair. Animatable Gaussians [65] uses a template that can fit outward appearance as guidance and leverages StyleGAN to learn the pose-dependent Gaussian maps, enhancing the capability for modeling detailed dynamic appearances. GaussianAvatar [61] employs a feature that captures the coarse global appearance, which is integrated with a pose feature. These combined features are then input into a decoder to predict parameters for Gaussian primitives. 3DGS-Avatar [63] introduces a non-rigid transformation module that utilizes a multi-level hash grid encoder to encode 3D position, and concatenates it with a pose latent to form the input for a shallow MLP network, which predicts offsets of Gaussian’s position, scale, and rotation under certain poses.

Furthermore, certain studies [60], [62] opt not to utilize this feature, thereby reducing the complexity of the deformation and facilitating faster rendering speeds. However, these approaches also introduce a degree of distortion.

*Some studies project the problem space from 3D to 2D, thereby reducing complexity and enabling the utilization of well-established 2D networks for parameter learning.*

ASH [64] proposes generating a motion-related template mesh via a deformation network and predicting a motion-related texture map from this mesh. Then, a 2D network predicts Gaussian parameters through the generated texture map. Similarly, Animatable Gaussians [65] projects a template mesh human model from canonical space onto two 2D planes, frontal and dorsal, learning Gaussian attributes in these spaces.

GPS-Gaussian [59] addresses the generalizable human novel view synthesis by introducing Gaussian Parameter Maps that can be directly regressed without per-subject optimizations. This approach is complemented by a depth estimation module that lifts 2D parameter maps into 3D space.

#### 4.1.2 Head Reconstruction

In the field of human head reconstruction, like most pipelines using SMPL as a strong prior, the work by GaussianAvatars [68] integrates FLAME [69] meshes to provide prior knowledge with 3DGS to achieve superior rendering quality. This method compensates for the fine details and elements that the FLAME mesh fails to accurately depict or track. Nevertheless, Gaussian Head Avatar [70] critiques the use of FLAME meshes and Linear Blend Skinning (LBS) for facial deformation, noting that these relatively simple linear operations struggle to capture the nuances of intricate facial expressions. Instead, it proposes employing a MLP to directly predict the displacement of Gaussians as they transition from a neutral to a target expression. This approach facilitates the rendering of high-resolution head images, achieving resolutions up to 2K.

#### 4.1.3 Others

Additionally, 3DGS has introduced innovative solutions in other human-related areas. GaussianHair [71] focuses on the reconstruction of human hair, using linked cylindrical Gaussian modeling for the strands. At the same time, it specifically introduces the GaussianHair Scattering Model to further enhance the capture of structures, allowing the reconstructed strands to render with high fidelity under different lighting conditions.

The research presented in Gaussian Shadow Casting for Neural Characters [72] focuses on shadow computation under various perspectives and movements, which first reconstructs the volume of density, normals, and albedo values from input human poses and training images using NeRF. Subsequently, it fits the NeRF output density maps with a collection of anisotropic Gaussians. The Gaussian representation enables more efficient ray tracing and deferred rendering techniques, replacing traditional sampling processes and thus accelerating the computation of shadows.

Additionally, some research [73], [74] has explored the integration of 3DGS with generative models, which will be discussed in Sec. 4.2.

## 4.2 Artificial Intelligence-Generated Content (AIGC)

Artificial Intelligence Generated Content (AIGC) leverages artificial intelligence technologies to autonomously produce content. Recently, there has been a surge in methodologies for generating 3D ( $XYZ$ ) representations based on 3DGS. In this chapter, we systematically classify contemporary algorithms based on the types of prompts and the objects they generate. The categories include Image-to-3D Object Generation, Text-to-3D Object Generation, Multi-Object and Scene Generation, and 4D Generation ( $XYZ - T$ ), as shown in Fig. 4. Below, we provide an overview of the relevant works within each of these categories.

### 4.2.1 Text to 3D Objects

At present, a substantial body of research is dedicated to extending Score Distillation Sampling (SDS) [79], which plays a crucial role in this context, aiming to directly generate 3D representations with multi-view consistency using a distillation paradigm. To further elucidate SDS, we denote the 3D representations as  $\theta$  and the differentiable rendering process as  $g(\cdot)$ , thereby representing the rendered image as  $g(\theta)$ . DREAMFUSION [79] ensures that the rendered images from each camera viewpoint adhere to the credible samples derived from the pre-trained diffusion model  $\varphi$ . In practice, they leverage the score estimation function  $\epsilon_\phi(\mathbf{x}_t, t, y)$  of the existing diffusion model, where  $\epsilon_\phi$  predicts the sampled noise based on the noisy image  $\mathbf{x}_t$  and the textual condition  $y$ . Therefore, the gradient of score distillation loss for  $\theta$ ,

$$\nabla_\theta = \mathbb{E} \left[ w_t (\epsilon_\phi(\mathbf{x}_t, t, y) - \epsilon) \frac{\partial \mathbf{x}}{\partial \theta} \right]. \quad (3)$$

Subsequent works have widely adopted this, or improved variations thereof, as the primary supervision for generation.

*Some works [75], [80], [81] focus on improving the framework to apply score distillation loss to 3DGS.*

DreamGaussian [75], an early work integrating diffusion models with 3DGS, utilizes a two-stage training paradigm. Building upon Score Distillation Sampling (SDS), this approach ensures the geometric consistency of the generated models by extracting explicit Mesh representations from the 3DGS and refines texture in the UV space to enhance the quality of the renderings. The work by Chen et al. [80], conducted contemporaneously, introduces Point-E [82] (or other text-to-point-cloud models), along with 3D score distillation loss, to guide the 3D geometry generation in the first stage. And in the second stage, a density-based densification is employed to further refine the generation quality. Similarly, GaussianDreamer [81] adopts the same fundamental concept; however, it distinguishes itself by employing strategies such as noise point growth and color perturbation to address the issue of insufficient point cloud density during the initialization.

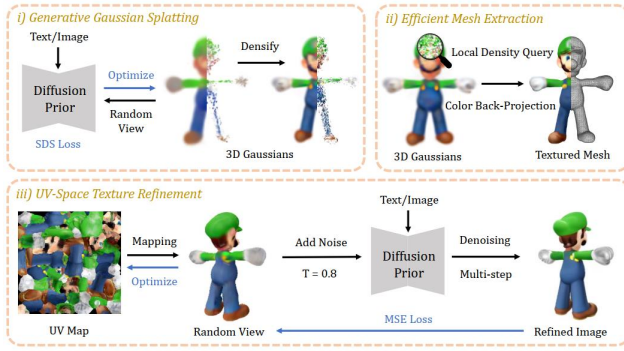
*However, the mode-seeking paradigm of score distillation frequently leads to oversaturation, excessive smoothing, and lack-detail in the generated outcomes, which has been extensively discussed in related works on NeRF [83].*

GaussianDiffusion [84] introduces variational Gaussian to mitigate the instability of 2D diffusion models and incorporates structured noise to enhance the 3D consistency.

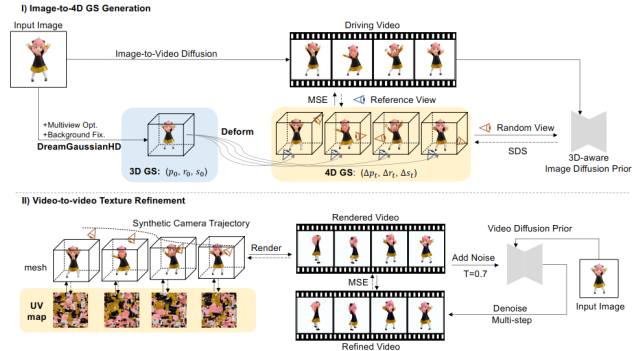
*There are also some works that focus on improving SDS.*

LucidDreamer [85] addresses the challenges of over-smoothing and insufficient sampling steps inherent in traditional SDS. By introducing deterministic diffusion trajectories (DDIM [86]) and interval-based score matching mechanisms Eq. 9, it achieves superior generation quality and efficiency. Subsequently, Hyper-3DG [87] builds upon LucidDreamer [85] by introducing a hypergraph [88] to explore the relationships between patchified Gaussian primitives.

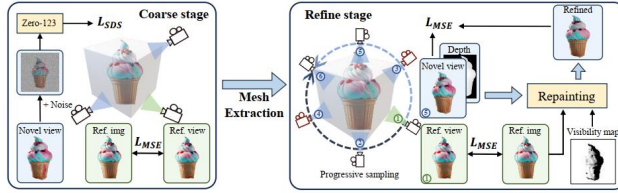
Similarly, LODS [89] analyzes the inherent inconsistency between the training and testing processes and the over-smoothing effect caused by large CFG (Classifier-Free Guidance) in SDS. To address these challenges, LODS proposes an additional set of learnable unconditional embeddings and



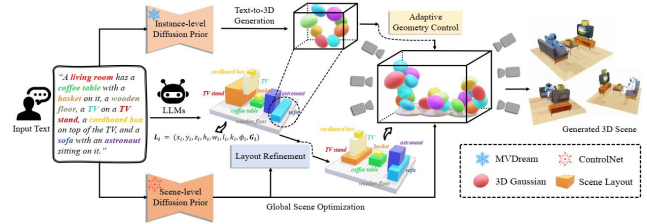
(a) Text to 3D Objects [75].



(b) 4D Generation [76].



(c) Image to 3D Object [77].



(d) Multi-Object Generation [78].

Fig. 4: Four typical tasks of 3DGC in AIGC Applications.

low-rank parameters of LoRA (Low-Rank Adaptation) [90] for aligning distributions.

*Score distillation loss can also be replaced in AIGC.*

IM-3D [91] identifies optimization difficulties associated with score distillation loss. Thus, it attempts to fine-tune existing image-to-video generation models to enable the generation of multi-view spatially consistent images (videos). These generated multi-view images are then used as supervision for 3DGS generation. Similarly, LGM [92] proposes a novel paradigm to generate 3DGS from text or a single image. It generates multi-view images of the target using existing networks and reconstructs 3D models under different inputs using an asymmetric U-Net based architecture with cross-view self-attentions.

*Works [93], [94] aim to generate using only feed-forward networks without the need for scene-specific training.*

BrightDreamer [93] aims to incorporate generalizable representation, as described in 3.3.1, into text-to-3D generation, enabling the direct creation of 3D models without the need for retraining in specific scenes. BrightDreamer predicts positional offset after fixed initialization and introduces a text-guided triplane generator for the extracted textual features to predict other attributes of 3DGS, thereby achieving the conversion of arbitrary text into 3D models. GVGGEN [94] focuses on a feed-forward setup without triplane, proposing GaussianVolumes as a structured lightweight representation for generalizable generation. Based on this representation, GVGGEN generates a Gaussian Distance Field with a trained diffusion model and utilizes it to guide the prediction of corresponding attributes.

*Some works [73], [74] also attempt to apply this generative paradigm to areas such as digital human generation.*

HumanGaussian [74] combines RGB and depth rendering to improve the SDS, thereby jointly supervising the opti-

mization of the structural perception of human appearance and geometry. Additionally, it introduces annealed negative prompt guidance and a scaling-based pruning strategy to address oversaturation and floating artifacts. In addition to the numerous works relying heavily on diffusion models, the work by Abdal et al. [73] proposes a novel paradigm that combines 3DGS with Shell Maps [95] and a 3D Generative Adversarial Networks (GANs) framework. By leveraging Gaussian Shell Maps, this approach rapidly represents human bodies and their corresponding deformations.

#### 4.2.2 Image to 3D Object

Similar to works on NeRF, recent studies [77], [96] have also focused on generating entire 3DGS from a single image.

Following a process similar to DreamGaussian [75], Repaint123 [77] divides this procedure into coarse and fine optimization stages. In the coarse stage, it uses the pre-trained Zero-123 [97] as supervision and employs SDS to optimize a coarse 3DGS. During the fine stage, Repaint123 extracts the mesh representation from the first stage and proposes combining depth and reference images to guide the denoising process on novel view images, ensuring consistency across views. For overlapping and occluded regions between views, Repaint123 employs visibility-aware adaptive repainting methods to enhance repainting quality in these areas, which are then used for fine-tuning 3DGS.

FDGaussian [96] proposes a more straightforward approach by dividing the entire generation process into multi-view image generation and 3DGS reconstruction. During the generation phase, FDGaussian extracts 3D features from the image by decoupling orthogonal planes, optimizing the multi-view generation model based on Zero-1-to-3 [97]. In the reconstruction phase, it enhances the efficiency and performance of 3DGS through control optimization based



on inter-Gaussian distances and a fusion strategy based on epipolar attentions.

#### 4.2.3 Multi-Object and Scene Generation

In addition to single-object generation, multi-object and scene generation is more crucial in most application scenarios.

**Multi-Object Generation:** Several studies [78], [98] have explored the generation of multiple composite objects, which not only *concentrate on the individual objects* but also aim to *investigate the interactions between multiple objects*.

CG3D [98] discusses both aspects separately. For the reconstruction of individual objects, CG3D introduces the  $K$  nearest neighbors loss on Alpha hull [99] to ensure that the predicted Gaussian primitives are uniformly distributed and concentrated on the object surfaces. For predicting the interactions between multiple objects, CG3D leverages SDS and probabilistic graph models extracted from text to predict the relative relationships between objects. Finally, by incorporating priors such as gravity and contact relationships between objects, CG3D achieves models with realistic physical interactions.

To simplify such a problem, GALA3D [78] uses layouts generated by large language models (LLMs) to guide multiple object reconstructions. By exploring the distribution of positions and optimizing the shapes of Gaussian primitives according to the layout, GALA3D generates scenes that conform to the specified layouts. Additionally, by supervising the generation of individual objects and entire scenes through SDS and introducing a Layout Refinement module, GALA3D achieves more realistic and text-consistent generation results.

**Scene Generation:** Unlike object-centric generation, scene generation often requires the incorporation of additional auxiliary information, such as pre-trained monocular depth estimation models, to achieve high-precision initialization.

To achieve this, LucidDreamer<sup>2</sup> [100] designs a two-stage generative paradigm. In the first stage, LucidDreamer<sup>2</sup> leverages pre-trained text-to-image models and monocular depth estimation models to initialize the point clouds, and introduces Stable Diffusion inpainting models [101] to complete a multi-view consistent scene point cloud. In the second stage, the generated point cloud is used to initialize 3DGS, with extended supervision images to ensure a smoother training process. Based on a similar paradigm, Text2Immersion [102] introduces a poses-progressive generation strategy to achieve a more stable training process, and incorporates enlarged viewpoints and pre-trained super-resolution models to optimize the generated scenes.

#### 4.2.4 4D Generation

In addition to static scenes, some studies [76], [103], [104] have begun to delve deeply into dynamic 3D scenes. Analogous to static scene generation using text-to-image SDS, *it is natural to consider that text-to-video SDS could potentially generate dynamic scenes*.

Align Your Gaussians (AYG) [103] explicitly divides the problem into two stages: static 3DGS reconstruction and 4DGS (dynamic 3DGS) reconstruction. In the static reconstruction stage, AYG incorporates the pre-trained text-guided multiview diffusion model MVDream [105] and text-to-image model to jointly supervise the 3DGS training. In the dynamic reconstruction stage, AYG proposes using

both pre-trained text-to-image and text-to-video models to supervise the dynamic 3DGS training. Moreover, AYG introduces a simplified score distillation loss to reduce training uncertainty.

Building on DreamGaussian [75], DreamGaussian4D [76] takes a single reference image as input and utilizes pre-trained image-to-video models as well as multi-view generation models for supervised training.

GaussianFlow [104] aims to use optical flow information from videos as auxiliary supervision to assist 4DGS creation. Similar to the dynamic Gaussian work, Motion4D [106], this study first analyzes the relationship between Gaussian primitives' movement in 3D space and pixel movement (optical flow) in 2D pixel space. By aligning the motion of 3D Gaussians with optical flow, GaussianFlow can achieve text-to-4DGS and image-to-4DGS generation.

*However, the instability of video generation models affects the generation performance in the SDS-based paradigm.*

4DGen [107] addresses this issue by introducing multi-view generation models for each frame of the given video to create pseudo-labels, replacing video generation models. To ensure temporal consistency, 4DGen utilizes multi-scale intermediate representations from Hexplane [108] to constrain the smoothness of Gaussian primitives over time, further enhancing 4DGS generation quality. Similarly, in the same context and experimental setup, Fast4D [109] forms a matrix of images using these pseudo-labels and considers continuity in both temporal and spatial dimensions (i.e., rows and columns). Using the image matrix as supervision, the Fast4D propose a novel time-dependent 3DGS representation [110] to achieve efficient and high-quality generation.

*Additionally, some studies [111] focus on animating existing static 3DGS.*

For animating existing 3DGS from input video, BAGS [111] introduces neural bones and skinning weights to describe the spatial deformation based on canonical space. Using diffusion model priors and rigid body constraints, BAGS can be manually manipulated to achieve novel pose rendering.

### 4.3 Autonomous Driving

In the field of autonomous driving, 3DGS is primarily applied to the dynamic reconstruction of large-scale driving scenes and combined SLAM applications.

#### 4.3.1 Autonomous Driving Scene Reconstruction

Reconstruction driving scenes is a challenging task, involving multiple technical domains such as large-scale scene reconstruction, dynamic object reconstruction, static object reconstruction, and Gaussian mixture reconstruction.

*A substantial body of works [112], [113], [114] categorizes the reconstruction process into static background reconstruction and dynamic target reconstruction.*

DrivingGaussian [112] aims to utilize multi-sensor data for reconstructing large-scale dynamic scenes in autonomous driving. In the static background, DrivingGaussian introduces incremental static 3D Gaussians under different depth bins to mitigate the scale confusion caused by distant street scenes. For dynamic objects, DrivingGaussian introduces dynamic Gaussian graphs to construct relationships among

multiple targets (whose attributes include position, local-to-world coordinate transformation matrices, and orientation, etc.), jointly reconstructing the entire autonomous driving scene with the static background. StreetGaussians [113] adopts a similar approach, with the key difference being the introduction of semantic attributes during the reconstruction of background and foreground. Also, StreetGaussians uses Fourier transforms to efficiently represent the SH’s temporal changes of dynamic 3DGS. Building on previous works, HUGS [114] incorporates the Unicycle Model and the modeling of forward and angular velocities to assist in the dynamic reconstruction under physical constraints. Similar to previous dynamic 3DGS efforts [106], [115], HUGS also employs optical flow supervision, combined with rendered RGB loss, semantic loss, and Unicycle Model losses, thus improving dynamic reconstruction accuracy.

*Moreover, 3DGS have been applied to multimodal spatiotemporal calibration tasks [116].*

By leveraging the LiDAR point cloud as a reference for the Gaussians’ positions, 3DGS-Calib [116] constructs a continuous scene representation and enforces both geometrical and photometric consistency across all sensors, achieving accurate and robust calibration with significantly reduced training times compared to NeRF-based methods.

#### 4.3.2 Simultaneous Localization and Mapping (SLAM)

SLAM is a fundamental problem in robotics and computer vision, where a device constructs a map of an unknown environment while simultaneously determining its own location within that environment. The technical approaches to SLAM can be broadly categorized into traditional methods, techniques involving NeRF, and approaches related to 3DGS. Among these, 3DGS methods stand out for their ability to offer continuous surface modeling, reduced memory requirements, improved noise and outlier handling, enhanced hole filling and scene repair, and flexible resolution in 3D mesh reconstruction [117].

*Some studies [118], [119], [120], [121], [122] have retained the traditional SLAM inputs and approached this from two perspectives: online tracking and incremental mapping.*

In earlier works, GS-SLAM [118] utilizes 3DGS as a scene representation for SLAM and introduces an adaptive expansion strategy. This strategy involves the dynamic addition of new Gaussian primitives during the training phase and the removal of noisy primitives based on captured depth and rendered opacity, thereby facilitating continuous scene reconstruction during motion. For camera tracking, GS-SLAM proposes an advanced coarse-to-fine optimizing strategy. Initially, a sparse set of pixels is rendered to optimize the tracking loss and obtain an initial, coarse estimate of the camera poses. Subsequently, based on these coarse camera poses and depth observations, reliable Gaussian primitives are selected in 3D space to guide GS-SLAM in re-rendering regions with well-defined geometric structures, which further refines the coarse camera poses. The entire process is supervised using a re-rendering loss.

Photo-SLAM [119] introduces a novel SLAM framework featuring a Hyper Primitives Map, which incorporates ORB features [123] along with Gaussian attributes. Based on such representation, this framework leverages the Levenberg-Marquardt (LM) algorithm [124] to optimize both the lo-

calization and geometric maps from projection relationships. Building on these results, Photo-SLAM proposes a geometry-based densification strategy and a Gaussian-Pyramid-Based Learning mechanism to construct photorealistic mapping. Finally, the framework integrates loop closure [123] to further correct camera poses and improve mapping quality.

Gaussian-SLAM [121] addresses the mapping challenge by dividing the map into multiple submaps, each reconstructed separately, thereby alleviating catastrophic forgetting. For camera tracking, the authors observe that tracking accuracy is constrained by the extrapolation capabilities of 3DGS and recommend incorporating trajectory assistance from DROID-SLAM [125] to enhance the reconstruction.

The work [126] analytically derives the Jacobian matrix concerning camera poses, proposing an efficient camera pose optimization strategy. During the mapping phase, the authors estimate frame-to-frame co-visibility and design a keyframe selection and management mechanism that prioritizes frames with low co-visibility as keyframes. This ensures the efficient use of non-redundant keyframes in the same region, thereby enhancing mapping efficiency.

Based on previous works, RGBD GS-ICP SLAM [127] integrates the Generalized Iterative Closest Point (G-ICP) [128] algorithm into the mapping and tracking. By sharing the covariances between G-ICP and 3DGS as well as employing scale alignment techniques, this work minimizes redundant computations and facilitates rapid convergence.

Similarly, the work by Sun et al. [129] also proposes a densification strategy guided by holes and rendering errors to map unobserved areas and refine re-observed regions. Additionally, the authors design a new regularization term to alleviate the problem of catastrophic forgetting.

*Semantics are important as they not only provide scene understanding but also stabilize the training process.*

SGS-SLAM [122] employs multi-channel geometric, appearance, and semantic features for rendering and optimization and proposes a keyframe selection strategy based on geometric and semantic constraints to enhance performance and efficiency. Furthermore, due to the construction of semantic representations, SGS-SLAM is capable of editing 3DGS, which correspond to semantically consistent regions. Based on it, SEMGAUSS-SLAM [130] designs a feature-level supervision for robustness and introduces a feature-based Bundle Adjustment to mitigate cumulative drift during tracking. Subsequent works, NEDS-SLAM [131], also adopts this concept, introducing semantic feature-assisted SLAM optimization and incorporating DepthAnything [132] to learn semantically rich features with 3D spatial awareness. Additionally, NEDS-SLAM proposes a novel pruning method based on virtual multi-view consistency checks to identify and eliminate outliers.

*Additionally, there are several works focusing on related issues such as localization [133] and navigation [134].*

3DGS-ReLoc [133] introduces a LiDAR data initialization to assist in 3DGS mapping. Building upon this, it proposes dividing the 3DGS submap into a 2D voxel map and utilizing a KD-tree for efficient spatial queries, thereby mitigating excessive GPU memory consumption. Finally, 3DGS-ReLoc employs a feature-based matching and Perspective-n-Point (PnP) method to iteratively refine the pose of the query image, achieving precise localization within the global map.

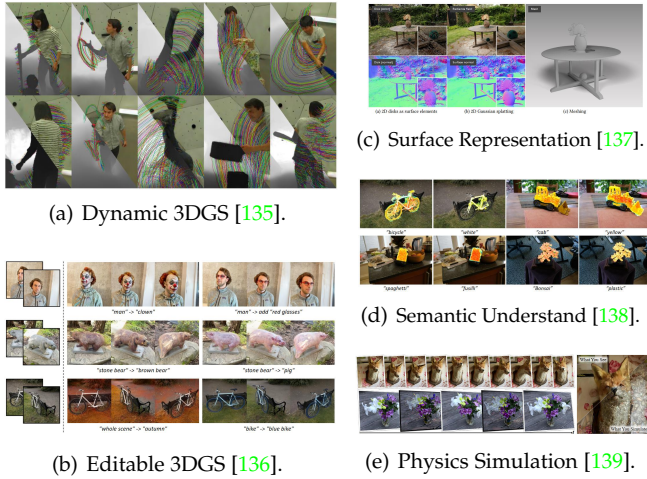


Fig. 5: Five different Extensions of 3DGC.

In the context of indoor navigation, GaussNav [134] focuses on the instance image navigation (IIN) task. Based on reconstructed 3DGS maps, GaussNav proposes an image target navigation algorithm, achieving impressive performance through classification, matching, and path planning.

## 5 EXTENSIONS OF 3D GAUSSIAN SPLATTING

As an essential technique for 3D representation, 3DGS can be further expanded for more capabilities, including dynamic 3DGS [Fig. 5(a)], surface representation from 3DGS [Fig. 5(c)], editable 3DGS [Fig. 5(b)], 3DGS with semantic understanding [Fig. 5(d)], and 3DGS-based physics simulation [Fig. 5(e)].

### 5.1 Dynamic 3D Gaussian Splatting

The study of dynamic 3DGS has recently garnered significant attention from researchers. The reconstruction of dynamic scenes transcends the limitations of static scene reconstruction and can be effectively applied to fields such as human motion capture and autonomous driving simulation. Unlike static 3DGS, dynamic 3DGS must account for consistency not only in the spatial dimension but also in the temporal dimension, ensuring continuity and smoothness over time. Here, we categorize them into Multi-view Videos and Monocular Video based on different reconstruction inputs.

#### 5.1.1 Multi-view Videos

*Some works [135], [140] attempted to directly construct dynamic 3DGS frame by frame.*

An early work [135] extends 3DGS from static to dynamic scenes by allowing the Gaussians to move and rotate over time while maintaining persistent attributes such as color, opacity, and size. The reconstruction is performed temporally online, where each timestep is initialized using the previous timestep’s representation. The first timestep acts as an initialization for optimizing all attributes, which are then fixed for subsequent timesteps except for those defining motion. Physical priors, including local rigidity, local rotational-similarity, and long-term local-isometry, regularize the motion and rotation of the Gaussians, as shown in Eq. 5-7. The authors also discuss the impact of factors such as similar background information and multi-view camera differences on reconstruction performance.

Similarly, 3DGStream [140] designs a two-stage training process for transformation predictions. In the first stage, it introduces Neural Transformation Cache and I-NGP [9] to reconstruct dynamic 3DGS. In the second stage, 3DGStream proposes an adaptive densification strategy, initializing new Gaussian positions by calculating gradients.

*Other works [141], [142] aim to achieve such performance by predicting deformations.*

SWAGS [141] introduces a window-based 4DGS, sampling videos into multiple windows to achieve long-term scene reconstruction. To ensure that the deformation degree within each window is as similar as possible, an adaptive window division method based on average flow is introduced. A dynamic MLP is then used to guide the optimization to focus on dynamic areas. On the basis of predictions from multiple sampled windows, SWAGS proposes using the consistency of overlapping frames from adjacent windows to design a self-supervised loss that fine-tunes the entire scene, thus eliminating temporal discontinuities from window divisions.

#### 5.1.2 Monocular Video

*Some monocular dynamic 3DGS works [106], [143], [144], [145], [146] tend to divide into two stages: canonical reconstruction and deformation prediction.*

The study [143] first reconstructs static 3DGS in the canonical space. Then, it takes the encoded positions and time  $t$  as inputs, outputting offsets in terms of positions, rotations, and scales. To mitigate overfitting issues caused by inaccurate poses, this work introduces an annealing smooth training paradigm, which incorporates linearly decaying Gaussian noise.

Building on this foundation, GauFRé [144] proposes a paradigm that decouples dynamic and static scene modeling, where the dynamic part utilizes a method similar to that of [143]. 4D-GS [145] introduces the multi-scale HexPlane [108] as the foundational representation to encode temporal and spatial information. To optimize the training process, 4D-GS employs multi-head decoders to predict different attributes of Gaussian primitives separately. MD-Splatting [146] also builds on this by incorporating the local rigidity loss and isometric loss as proposed in [135], and designs a regularization term based on the law of conservation of momentum, making the dynamic motion trajectories smoother. Additionally, the authors include shadow prediction in the decoding part, further enhancing the realism of the reconstruction.

The work by Guo et al. [106] constructs a flow-augmentation method by analyzing the correspondence between 3D Gaussian motion and pixel-level flow, introducing additional optical flow-based supervision based on uncertainty and dynamic awareness. Additionally, it proposes a Motion Injector and Dynamic Map Refinement strategy based on a velocity field to mitigate the challenges associated with predicting deformations.

*Instead of discrete offsets, exploring temporally continuous motion can promote smoothness in the time dimension.*

The work by Katsumata et al. [115] incorporates Fourier approximations over time and optical flow supervision to model the attribute changes of 3DGS, ensuring continuous changes without introducing excessive parameters.

DynMF [147] argues that every scene is comprised of a limited fixed number of trajectories and introduces efficient basis functions for spatial motion. Based on these basis functions, DynMF designs motion coefficients to predict dynamic positions and rotation attributes, and introduces constraints such as sparsity and rigidity to further enhance optimization performance. Similarly, STG [148] proposes the use of temporally relevant Radial Basis Functions to represent the opacity attributes, and utilizes parameterized polynomials to describe the motion and rotation of Gaussian primitives. Additionally, a new time- and view-dependent feature splatting paradigm is introduced to replace spherical harmonics for color.

Gaussian-Flow [149] aims to develop a representation capable of fitting variable motion by analyzing the advantages and disadvantages of polynomial [147], [148] and Fourier series fitting [115]. It then proposes a model that combines both methods to construct a dual-domain deformation prediction model. Finally, Gaussian-Flow introduces an adaptive time-step scaling strategy and a temporal smoothing and rigid loss to enhance training stability and temporal continuity.

SC-GS [150] aims to compress motion representations in dynamic scenes based on sparse control points. By predicting the positions of control points, radial-basis-function (RBF) kernels, and transformations, the motion of the entire dynamic field over time is calculated using the Linear Blend Skinning [151]. Thanks to this strategy, SC-GS proposes an adaptive pruning and cloning strategy for control points based on neighboring point RBF weights and gradients, and it demonstrates strong applicability in 3DGS editing.

*Recent works [110], [152] aim to extend 3DGS to 4D space for dynamic 3D scenes representation.*

The work [110] achieves end-to-end training by incorporating the time dimension into the 3D representation directly. The core idea is to simultaneously consider spatial variables ( $XYZ$ ) and time variable ( $T$ ) along with their interrelations, rather than treating them as independent variables. For 4D Gaussian primitives, it designs a 4D representation of the rotation matrix  $\mathbf{R} \in \mathbb{R}^{4 \times 4}$  and scaling factor  $\mathbf{S}$  (4D diagonal), and employs 4D spherical harmonics to further describe the color variations over time.

Similarly, the work [152] proposes a rotor-based 4D Gaussian Splatting (4DGS) representation, wherein the rotation attributes of 4DGS are expressed by decomposing 4D rotors into eight components. These components, along with corresponding parameters, are used to describe the rotation in space-time. When representing dynamic 3DGS, it slices 4DGS at different timestamps, effectively addressing the sudden appearance or disappearance of objects in highly dynamic scenes. Furthermore, the approach enforces consistency in 4D space through the introduction of a 4D Consistency Loss.

## 5.2 Surface Representation

Although 3DGS enables highly realistic rendering, extracting surface representations remains challenging. After the optimization process, the resulting representations often lack ordered structures and do not correspond well to the actual surfaces. However, mesh-based representations remain the preferred choice in many workflows, as they allow the use of robust tools for editing, sculpting, animation, and relighting.

*When it comes to surface reconstruction, Signed Distance Functions (SDF) are an indispensable topic.*

NeuSG [153] attempts to jointly optimize NeuS [154] and 3DGS and introduces several regularization terms, including Scale Regularization, Normal Regularization, and Eikonal Regularization [155], to ensure that the 3DGS are as flat as possible and distributed along the target surface.

SuGaR [156] leverages the 3DGS surface characteristics to design an idealized SDF. This idealized representation is then used to constrain the actual predicted SDF and its normals, thereby encouraging the optimized Gaussians to more closely align with the object's surface. Then, using Poisson reconstruction, SuGaR extracts a mesh from the aligned 3DGS, which is faster and more scalable than the Marching Cubes algorithm [157]. Additionally, an optional refinement step binds new Gaussians to mesh and jointly optimizes them, enabling high-quality rendering and surfaces.

And then, 3DGSR [158] aims to integrate neural implicit SDF with 3DGS by designing a differentiable SDF-to-opacity transformation function, enabling the optimization of 3DGS to update the SDF. To address the challenge of optimizing continuous SDF with discrete 3DGS, 3DGSR proposes enforcing consistency between the depth (normals) obtained from volumetric rendering and those inferred from 3DGS.

GSDf [159] similarly introduces consistency constraints and employs a dual-stream network combining 3DGS and neural implicit SDF based on Scaffold-GS [26] and NeuS [154]. To improve the sampling efficiency of SDF, GSDf uses the depth maps from the 3DGS branch to guide the ray sampling process, and to improve the distribution of Gaussian primitives on surfaces, designs a Geometry-aware Gaussian Density Control for 3DGS based on the SDF branch.

*Other studies [137], [160], [161] aim to address this issue by enhancing the intrinsic attributes of 3DGS.*

The work [160] introduces a novel representation termed Gaussian Surfels, which exhibits an enhanced capability for surface reconstruction. Based on this representation, it proposes a depth-normal consistency loss to address the gradient vanishing problem and a volumetric cutting strategy to prune unnecessary voxels in regions with depth errors and discontinuities. Finally, this work applies screened Poisson reconstruction to generate the surface mesh.

Gaussian Opacity Fields (GOF) [161] are developed based on 3DGS, wherein 3DGS is normalized along the ray to form a 1DGS for volume rendering. GOF also incorporates depth distortion and normal consistency losses, facilitating the extraction of surface meshes from tetrahedral grids.

Similarly, 2D Gaussian Splatting [137] (2DGS) replaces 3DGS with planar disks to represent surfaces, which are defined within the local tangent plane. In the rendering process, 2DGS abandons direct affine transformations and uses three non-parallel planes to define the ray-splat intersections, followed by rasterization after applying a low-pass filter.

## 5.3 Editable 3D Gaussian Splatting

3DGS, with its advantages of real-time rendering, representation of complex scenes, and explicit representation, has naturally attracted considerable attention from researchers focusing on 3DGS editing. Unfortunately, current editable 3DGS works often lack precise training supervision, which

poses a significant challenge for editing. In this section, we categorize existing works according to different tasks.

### 5.3.1 Manipulation by Text

To address this challenge, the existing works can be classified into two distinct categories. *The first type introduces the score distillation loss as in Eq. 3.* Unlike AIGC 4.2, these methods require editing prompts as additional conditions to guide the editing process.

Based on the SDS, GaussianEditor [162] introduces semantic control into 3DGS editing, enabling semantic-based tracking and automatic masking of editing regions. More importantly, this work proposes a hierarchical 3DGS and multi-generation anchor loss, which stabilizes the editing process and mitigates the SDS’s impact of randomness. Additionally, GaussianEditor introduces 2D inpainting techniques to provide guidance for the tasks of object removal and incorporation. Following Dreamgaussian [75], GSEdit [163] uses the pre-trained Instruct-Pix2Pix [164] model instead of the image generation model to compute score distillation loss for 3DGS editing.

*The second type focuses on sequentially editing multi-view 2D images before reconstructing 3DGS.*

GaussianEditor<sup>2</sup> [165] leverages multi-modal models, large language models, and segmentation models to predict the editable regions from given textual descriptions. It then optimizes the relevant Gaussian primitives within the target regions based on the images edited by the 2D editing models.

*However, such a paradigm introduces an intuitive problem: how to ensure consistency in multi-view editing.*

GaussCtrl [166] introduces a depth-guided image editing network, ControlNet [167], utilizing its ability to perceive geometry and maintain multi-view consistency in the editing network. It also introduces a latent code alignment strategy in the attention layers, ensuring that the edited multi-view images remain consistent with the reference images.

The work [136] aims to introduce inverse rendering and rendering in 3D latent space to maintain consistency on the attention map. Furthermore, it introduces an editing consistency module and an iterative optimization strategy, further enhancing the multi-view consistency and editing capabilities.

*Unlike editing methods for 3DGS, recent discussions have increasingly focused on editing 4DGS.*

Recent work, Control4D [168], delves into this area by introducing 4D GaussianPlanes, which structurally decompose the 4D space to ensure consistency across spatial and temporal dimensions as Tensor4d. Based on the GaussianPlanes, it designs a 4D generator using super-resolution generative adversarial networks [169], which learns a generation space on GaussianPlanes from the edited images generated by the diffusion model and employs a multi-stage progressive guiding mechanism to enhance the local-global quality.

### 5.3.2 Manipulation by Other Conditions

In addition to text-controlled editing, existing works have explored 3DGS editing methods under various conditions. TIP-Editor [170] requires the provision of an editing text, a reference image, and the editing location to finely control 3DGS. The core technologies include a stepwise 2D personalization strategy for learning the existing scene and the

new content separately, and a coarse-fine editing strategy for accurate appearance. This approach allows users to perform various editing tasks, such as object insertion and stylization.

Point’n Move [171] requires the user to provide annotated points for the objects to be edited. It achieves controlled editing (including inpainting the removal area) of the objects through dual-stage segmentation, inpainting, and recomposition steps.

### 5.3.3 Stylization

In the realm of style transfer for 3DGS, early explorations have been made by [172]. Similar to traditional style transfer works [173], this work designs a 2D stylization module on the rendered images and a 3D color module on the 3DGS. By aligning the stylized 2D results of both modules, this approach achieves multi-view consistent 3DGS stylization without altering the geometry.

### 5.3.4 Animation

As described in 5.1, some dynamic 3DGS works, such as SC-GS [150], can achieve animation effects by animating sparse control points. AIGC-related works, such as BAGS [111], aim to utilize video input and generation models to animate existing 3DGS. Similar research has also been mentioned in the context of Human Reconstruction.

Additionally, CoGS [174] discusses how to control this animation. Based on dynamic representations [135], [143], it uses a small MLP to extract relevant control signals and align the deformation of each Gaussian primitive. And then, CoGS generates 3D masks for the regions to be edited to reduce unnecessary artifacts.

## 5.4 Semantic Understanding

Endowing 3DGS with semantic understanding capabilities allows for the extension of 2D semantic models into 3D space, thereby enhancing the model’s comprehension in 3D environments. This can be applied to various tasks such as 3D detection, segmentation, and editing.

*Many works attempt to leverage pre-trained 2D semantic-aware models for extra supervision on semantic attributes.*

Early work, Feature 3DGS [175], distills pre-trained 2D foundational models to jointly construct 3DGS and feature fields. By introducing a parallel feature rasterization strategy and regularization, it endows the 3DGS with the capability of spatial understanding and enables the design of Promptable Explicit Scene Representations for downstream tasks.

Subsequently, Gaussian Grouping [176] introduces the concept of Gaussian groups and extends Identity Encoding attributes to achieve it. This work proposes treating multi-view data as a video sequence with gradually changing views and utilizes a pre-trained object tracking model [177] to ensure multi-view consistency of the segmentation labels obtained from SAM (Segment Anything) [178]. Additionally, Gaussian groups are supervised in both 2D and 3D spaces and applied directly for editing. Similarly, the work [179] addresses semantic inaccuracy by introducing KNN clustering and Gaussian filtering, which can constrain nearby Gaussians and eliminate distant Gaussians.

CoSSegGaussians [180] leverages a pre-trained point cloud segmentation model in conjunction with a dual-stream

feature fusion module. This module integrates unprojected 2D features derived from 2D encoders with 3D features from 3D encoders, following the prediction of Gaussian locations [15]. By employing decoders and semantic supervision, CoSSegGaussians effectively imbues Gaussian primitives with semantic information.

Others [138], [181], [182] focus on incorporating text-visual alignment features for open-world understanding.

A significant challenge is the high dimensionality of CLIP features, which makes direct training and storage difficult compared to original Gaussian attributes. The work [138] introduces corresponding continuous semantic vectors into the 3DGS by extracting and discretizing dense features from CLIP [183] and DINO [184], which are used to predict semantic indices  $m$  in Discrete Feature Space by MLPs as in VQ-VAE [185]. It also proposes incorporating an uncertainty attribute to describe the instability and frequent changes of Gaussian primitives and designing an adaptive spatial smoothing loss to deliberately decrease the spatial frequency of the embedded compact semantic features.

LangSplat [181] compresses scene-specific CLIP features using a trained autoencoder to reduce training memory requirements. To achieve this objective, LangSplat introduces hierarchical semantics—subparts, parts, and wholes—constructed using SAM [178], which addresses point ambiguity across multiple semantic levels and facilitates scene understanding in response to arbitrary text queries. Subsequently, FMGS [182] mitigates the issue of large CLIP feature dimensions by introducing multi-resolution hash encoders [9].

### 5.5 Physics Simulation

Recent efforts aim to extend 3DGS to simulation tasks. Based on the "what you see is what you simulate" philosophy, PhysGaussian [139] reconstructs a static 3DGS as the discretization of the scene to be simulated, and then incorporates continuum mechanics theory along with the Material Point Method (MPM) [186] solver to endow 3DGS with physical properties. To stabilize rotation-based varying appearances and fill particles into the void internal region, PhysGaussian proposes an evolving orientation and internal filling strategy.

## 6 TECHNICAL CLASSIFICATION

3DGS can generally be divided into the following stages, as illustrated in Fig. 3: initialization, attribute optimization, splatting, regularization, training strategy, adaptive control, and post-processing. Additionally, some concurrent works aim to incorporate supplementary information and representations, thereby enhancing the capability of 3DGS. These technical improvements not only enhance the rendering performance of the original 3DGS but also address specific tasks in derivative works. Consequently, this section delves into the technological advancements in 3DGS, with the aim of providing valuable insights for researchers in related fields.

### 6.1 Initialization

Proper initialization has been shown to be crucial, as it directly affects the optimization process [187]. The initialization of 3DGS is typically performed using sparse points derived from Structure-from-Motion (SfM) or through random

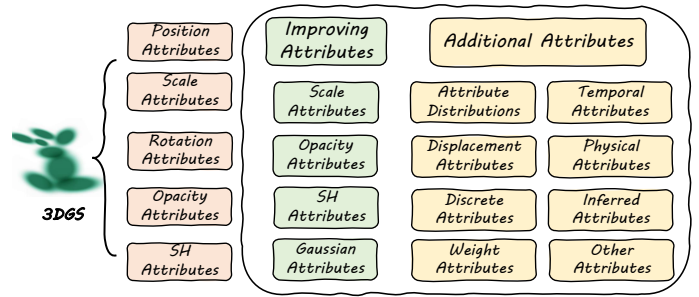


Fig. 6: Overview of Attribute Expansion Strategies.

generation. However, these methods are often unreliable, especially under weak supervision signals, such as sparse view settings and generative tasks.

*Combining pre-trained models is an optional approach.*

Pre-training a 3D model on a limited number of 3D samples and using it as an initialization prior is a viable strategy [51]. This approach can enhance the performance of initialization to some extent, although its effectiveness is contingent upon the data used. To address this limitation, pretrained 3D generative models [80], [81], [87] or monocular depth estimation models [100], [102] are also introduced for initialization purposes. Additionally, some works [80] propose the introduction of new perturbation points to achieve a more comprehensive geometric representation.

*Improving initialization strategies is also important.*

Based on the analysis of the role of SfM in capturing low-frequency signals within the spectrum, Sparse-large-variance (SLV) initialization is designed to effectively focus on the low-frequency distribution identified by SfM [187].

*Utilizing other representations can also enhance initialization capabilities.* By determining the Local Volumes from a coarse parametric point model, a small number of Gaussians are initialized within each volume, thereby avoiding excessive assumptions about the target [188]. Subsequently, an initialization strategy based on Visual Hull is proposed, enabling the acquisition of structural priors from four images [57].

**Discussion:** Precise initialization has the potential to benefit various derivative works of 3DGS by enhancing performance and ensuring a stable training process.

### 6.2 Attribute Expansion

The original attributes of 3DGS include position, scale, rotation, Spherical Harmonic (SH) coefficients, and an opacity value. Some works have extended these attributes to make them more suitable for downstream tasks. It can be categorized into improvements of existing attributes or the introduction of novel attributes, as shown in Fig. 6.

#### 6.2.1 Improving Attributes

*Certain attributes of Gaussian can be custom-tailored, thereby making 3DGS suitable for a wider range of tasks.*

**Scale:** By collapsing the  $z$ -scale to zero and incorporating additional supervision on depth, normal, or shell maps, the works [32], [73], [137], [156], [160] aim to improve Gaussian primitives to make them flatter and more suitable

for surface reconstruction, thereby mitigating inaccuracies in Gaussian geometric reconstruction. The  $z$  direction can be approximated as the normal direction. Similarly, a scale constraint, which limits the ratio of the major axis length to the minor axis length [116], [126], [139], ensures that the Gaussian primitives remain spherical to mitigate the issue of unexpected push artifacts caused by overly skinny kernels.

**SH:** By combining hash grids and MLP, the corresponding color attributes are encoded, effectively addressing the storage issues caused by a large number of SH parameters [23].

**Opacity:** By constraining the transparency to approach either 0 or 1, thereby minimizing the number of semi-transparent Gaussian primitives, the works [37], [156] achieve clearer Gaussian surfaces, effectively alleviating artifacts.

**Gaussian:** By introducing shape parameters, an attempt is made to replace the original Gaussians with a Generalized Exponential (GEF) mixture [27]. Traditional 3DGS can be viewed as a special case of the Generalized Exponential Family (GEF) mixture ( $\beta = 2$ ), enhancing the representational efficiency of Gaussians,

$$\hat{G}(x) = \exp \left\{ -\frac{1}{2} \left( (x - \mu)^\top \Sigma^{-1} (x - \mu) \right)^{\frac{\beta}{2}} \right\}. \quad (4)$$

### 6.2.2 Additional Attributes

*By adding new attributes and supervisions, the original representation capabilities of 3DGS can be augmented.*

**Semantic Attributes:** By introducing semantic attributes and corresponding supervision, works, such as [113], [114], [122], [130], [131], [175], are endowed with enhanced spatial semantic awareness, which is crucial for tasks such as SLAM and editing. After the splatting process used for semantic attributes, the 3DGS’s semantic attributes are supervised using 2D semantic segmentation maps. Additionally, improving methods for extracting semantic information [171] and introducing high-dimensional semantic-text features, such as CLIP and DINO features [138], [181], [182], have been employed to address a wider range of downstream tasks. Similar to semantic attributes, the Identity Encoding attributes can group 3DGS that belong to the same instance or stuff, which is more effective for multi-object scenes [176].

**Attribute Distributions:** Learning a distributed attribute with reparameterization techniques instead of a fixed value is an effective approach to prevent local minima in 3DGS [84] and mitigate its reliance on Adaptive Control of 3DGS [47]. In addition to these works focusing on the distribution prediction of position attributes, the distribution of scale attributes has also been incorporated [84]. By sampling the predicted attribute distributions, Gaussian primitives for splatting can be obtained.

**Temporal Attributes:** Replacing the original static attributes with temporal attributes is key to animating the 3DGS [109], [110], [113], [152]. For 4D attributes, including rotation, scale, and position, existing works render 3DGS on timestep  $t$  by either taking time slices at specific time points [152] or decoupling the  $t$  dimension from 4D attributes [109], [110]. Also, the introduction of 4D SH is crucial for time-varying color attributes. For this, the Fourier series is typically used as the adopted basis functions to endow SH with temporal capabilities in existing works [110], [113].

Note that due to involving different timesteps, such attributes often require video-based training.

**Displacement Attributes:** Displacement attributes are indispensable as they describe the relationship between the final and initial positions of Gaussian primitives. These attributes can be classified based on their dependency on time. Time-independent displacement attributes are often used to correct coarse position attributes, which can be directly optimized in the same manner as other attributes [46], [63]. Time-dependent displacement attributes can describe the positional changes of static 3DGS, thereby achieving dynamic representations. This approach often involves introducing a small MLP to predict displacement based on timestep  $t$  [143], [144], [145] and other control signals [174].

**Physical Attributes:** Physical attributes encompass a broad range of potential properties that describe the objective physical laws governing Gaussian primitives, thereby endowing 3DGS with more realistic representation. For instance, shading-related attributes such as diffuse color, direct specular reflection, residual color, and anisotropic spherical Gaussian can be utilized for specular reconstruction [37], [38], [39]. Additionally, shadow scalar is introduced to express shadows [146], and velocity is employed to represent the transient information of Gaussian primitives, which is essential for describing dynamic properties [106]. These attributes are typically updated by considering the influence of physical properties at specific rendering positions [37], [39], [146] or by incorporating supplementary supervised information, such as flow maps [106].

**Discrete Attributes:** Utilizing discrete attributes in place of continuous attributes is an effective method for compressing high-dimensional representations or representing complex motion. This is often achieved by storing the index values of the VQ codebook [17], [18], [19], [23] or the motion coefficient for motion basis [147] as the discrete attributes of Gaussian primitives. However, discrete attributes can lead to performance degradation; combining them with compressed continuous attributes may be a potential solution [138].

**Inferred Attributes:** This type of attribute does not require optimization; they are inferred from other attributes and used for downstream tasks. The Parameter-Sensitivity Attribute reflects the impact of parameter changes on reconstruction performance. It is represented by the gradient of the parameter and is used to guide compression clustering [19]. The Pixel-Coverage attribute determines the relative size of Gaussian primitives at the current resolution. It is related to the horizontal or vertical size of the Gaussian primitives and is used to guide the Gaussian’s scale to meet the sampling requirements of multi-scale rendering [34].

**Weight Attributes:** The Weight Attributes rely on structured representations, such as Local Volumes [188], Gaussian-kernel RBF [150], and SMPL [189], which determine the attributes of query points by calculating the weights of related points.

**Other Attributes:** The *Uncertainty Attributes* can help maintain training stability by reducing the loss weight in areas of high uncertainty [55], [138]. And, the *ORB-Features Attributes*, extracted from image frames [123], play a crucial role in establishing 2D-to-2D and 2D-to-3D correspondences [119].

**Discussion:** The modification of Gaussian attributes

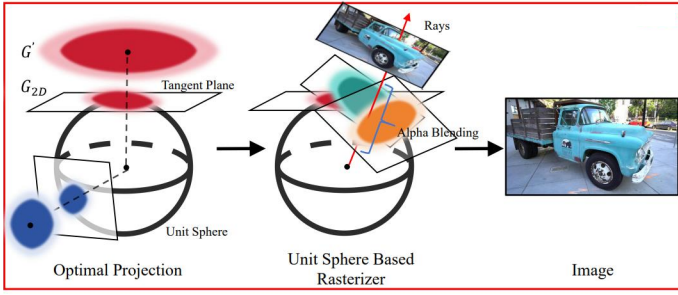


Fig. 7: The Modified Splatting Strategy [190].

facilitates the execution of a wider range of downstream tasks, offering an efficient approach as it obviates the need for additional structural elements. Moreover, the integration of new Gaussian attributes with supplementary information constraints also has the potential to significantly enhance the representational efficacy of the original 3DGS. For instance, semantic attributes can, in certain scenarios, yield more precise object boundaries.

### 6.3 Splatting

The role of Splatting is to efficiently transform 3D Gaussian data into high-quality 2D images, ensuring smooth, continuous projections and significantly improving rendering efficiency. As a core technology in traditional computer graphics, there are also efforts aimed at improving it from the perspectives of efficiency and performance [137].

Introducing the ADOP [12] in 3DGS for real-time rendering, TRIPS [191] utilizes a screen-space image pyramid for point rasterization and employs trilinear write for rendering large points. This approach, combined with front-to-back alpha blending and a lightweight neural network for detail reconstruction, ensures crisp, complete, and alias-free images.

The work [190] identifies limitations in prior methods [15] that use local affine approximations during the projection process, resulting in errors detrimental to rendering quality. By analyzing the residual errors from the first-order Taylor expansion, they establish a correlation between these errors and the Gaussian mean position. Based on this analysis, the unified projection plane is replaced with tangent planes, mitigating the projection errors in the original 3DGS through the Unit Sphere Based Rasterizer, as shown in Fig. 7. A similar issue is also mentioned in 2D-GS [137], which is introduced in Sec. 5.2.

### 6.4 Regularization

Regularization is crucial for 3D reconstruction. However, due to the lack of direct supervision from 3D data, the original 3DGS supervises its training by comparing the rendered images with the real images. This form of supervision can lead to training instability, particularly in under-determined scenarios such as those with sparse view settings. In this section, we categorize the regularization terms into 2D and 3D regularization terms, as shown in Fig. 8. The 3D regularization primarily provides constraints for 3DGS directly, whereas the 2D regularization terms impose

constraints on the rendered images, thereby influencing the optimization of attributes.

#### 6.4.1 3D Regularization

The 3D regularization has garnered significant attention due to its intuitive constraint capabilities. These efforts can be categorized based on their targeted objectives into individual Gaussian primitive, local, and global regularization.

**Individual Gaussian Primitive Regularization:** This regularization primarily aims to improve certain attributes of Gaussian primitives [32], [78], [126], [139], as mentioned in Sec. 6.2.

**Local Regularization:** Owing to the explicit representation of 3DGS, it is meaningful to impose constraints on Gaussian primitives within local regions. Such constraints can ensure the continuity of Gaussian primitives in the local space. *Physics-related Regularization* is often used to ensure the local rigidity of deformable targets, which includes short-term local-rigidity loss, local rotation similarity loss, and long-term local isometry loss. Short-term local rigidity implies that nearby Gaussians should move following a rigid body transformation between time steps,

$$\mathcal{L}_{i,j}^{\text{rigid}} = w_{i,j} \left\| \left( \boldsymbol{\mu}_{j,t-1} - \boldsymbol{\mu}_{i,t-1} \right) - \mathbf{R}_{i,t-1} \mathbf{R}_{i,t}^{-1} \left( \boldsymbol{\mu}_{j,t} - \boldsymbol{\mu}_{i,t} \right) \right\|_2, \quad (5)$$

where  $\boldsymbol{\mu}$  is Gaussian mean position,  $i$  and  $j$  are indexing of neighboring points,  $t$  is timestep, and  $\mathbf{R}$  represents rotation; Local rotation similarity enforces that adjacent Gaussian primitives have the same rotation over time steps,

$$\mathcal{L}_{i,j}^{\text{rot}} = w_{i,j} \left\| \hat{\mathbf{q}}_{j,t} \hat{\mathbf{q}}_{j,t-1}^{-1} - \hat{\mathbf{q}}_{i,t} \hat{\mathbf{q}}_{i,t-1}^{-1} \right\|_2, \quad (6)$$

where  $\hat{\mathbf{q}}$  is the normalized quaternion representation of each Gaussian's rotation; Long-term local isometry loss prevents elements of the scene from drifting apart,

$$\mathcal{L}_{i,j}^{\text{iso}} = w_{i,j} \left| \left\| \boldsymbol{\mu}_{j,0} - \boldsymbol{\mu}_{i,0} \right\|_2 - \left\| \boldsymbol{\mu}_{j,t} - \boldsymbol{\mu}_{i,t} \right\|_2 \right|, \quad (7)$$

[103], [104], [135], [146], [147], [150], [174], [188]. Subsequently, some works have also adopted similar paradigms to constrain local rigidity [111], [149].

In addition to rigidity loss, *Conservation of Momentum Regularization* can also be used as a constraint for dynamic scene reconstruction. It encourages a constant velocity vector and applies a low-pass filter effect to the 3D trajectories, thereby smoothing out trajectories with sudden changes [146]. In addition, there are some *Local Consistency Regularization* terms that also aim to constrain the Gaussian primitives within local regions to maintain similar attributes, such as semantic attributes [138], [176], [179], position [98], [107], time [149], frame [141], normal [192] and depth [52].

**Global Regularization:** Unlike the local regularization within neighboring regions, global regularization aims to constrain the overall 3DGS. *Physics-related Regularization* introduces real-world physical characteristics to constrain the state of 3DGS, including gravity loss and contact loss, among others. Gravity loss is used to constrain the relationship between the object and the floor, while contact loss targets the relationships among multiple objects [98].



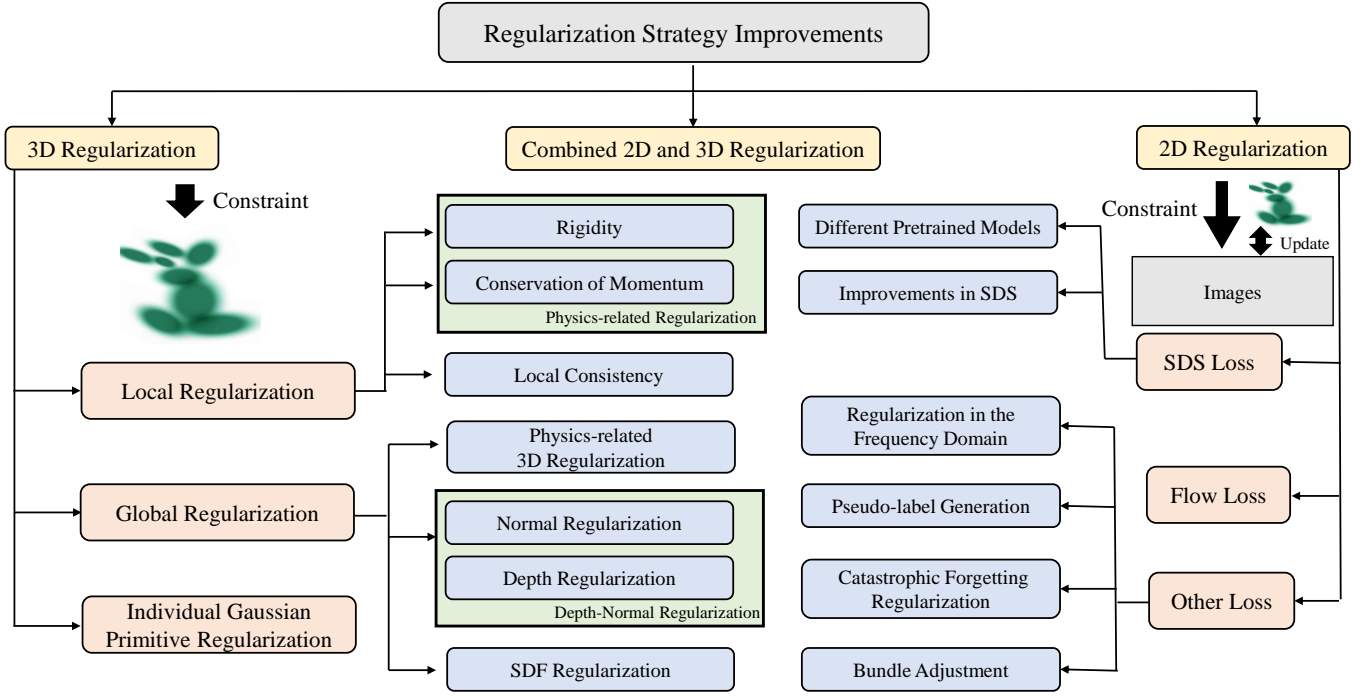


Fig. 8: Overview of Regularization Strategy Improvement in existing works.

Benefiting from the explicit representation of 3DGS, depth and normal direction attributes can be directly obtained, which can serve as constraints during training, particularly for surface reconstruction tasks. *Depth-Normal Regularization* achieves depth-normal consistency by comparing the normal computed from the depth values with the predicted normal [37], [158], [160], [161]. This method effectively enforces constraints on both normal and depth simultaneously. Additionally, directly constraining either the normal or the depth is also feasible. *Normal Regularization* often adopts a self-supervised paradigm due to the lack of direct supervision signals, which can be implemented by designing pseudo-labels from Gradient [153], Shortest axis direction of Gaussian primitives [37] or SDF [158], [159]. Similarly, *Depth Regularization* also adopts a similar approach; however, it not only aims for accurate depth values but also seeks to ensure clear surfaces in 3DGS. Depth Distortion loss [8] aggregates Gaussian primitives along the ray,

$$\mathcal{L}_d = \sum_{i,j} \omega_i \omega_j |z_i - z_j|, \quad (8)$$

where  $z$  is the intersection depth of Gaussian [137], [161]. In addition to self-supervised methods, incorporating additional pre-trained models to estimate normal [160] and depth [38], [54], [56], [193] has proven to be more effective in *Normal Regularization* and *Depth Regularization*. Based on them, derived works introduce hard depth and soft depth regularization to address the geometry degradation and achieve more complete surfaces [56]. A similar regularization term is *SDF Regularization*, which is also a constraint strategy for surface reconstruction. It achieves the desired surface by constraining the SDF that corresponds to 3DGS to an ideal

distribution [153], [156], [158], [159], [194].

#### 6.4.2 2D Regularization

Unlike the intuitive constraints of 3D regularization, 2D regularization is often used to address under-constrained situations where original loss functions alone are insufficient.

**SDS loss:** An important example is the SDS loss, as shown in Eq.3, which leverages a pre-trained 2D diffusion model to supervise 3DGS training through distillation paradigms [75], [162]. This approach is also extended to distill pre-trained 3D diffusion models [82], multi-view diffusion models [195], image editing models [164], and video diffusion models. Among these, the introduction of 3D diffusion models [80], [196] and multi-view diffusion models [76], [77], [78], [103], [104], [107] can optimize the reconstruction of explicit geometry and multi-view consistency. Image editing models [163] can achieve controllable editing, while video diffusion models [103] can be used for dynamic temporal scene generation with video SDS. Based on this paradigm, the distillation of other modal images also holds potential, as it can provide more constraints from corresponding pre-trained diffusion models, such as RGB-Depth [74], where designers need to discuss how to construct diffusion models.

Some improvements specifically target inherent issues in SDS [85], [89]. Interval Score Matching is proposed to address issues of randomness and single-step sampling,

$$\nabla_{\theta} \mathcal{L}_{\text{ISM}}(\theta) := \mathbb{E}_{t,c} \left[ \omega(t) (\epsilon_{\phi}(\mathbf{x}_t, t, y) - \epsilon_{\phi}(\mathbf{x}_s, s, \theta)) \frac{\partial g(\theta, c)}{\partial \theta} \right], \quad (9)$$

where  $s = t - \delta_T$  and  $\delta_T$  denotes a small step size [85]. Introducing Negative Prompts [197] is also a method [74],

[85], [196] to mitigate the impact of random noise  $\epsilon$  and enhance stability, by replacing random noise with negative prompts terms  $[\epsilon_\phi(\mathbf{x}_t; y_{\text{neg}})]$ . Subsequently, LODS introduces LoRA [90] terms  $[\frac{(1-w)\epsilon_{\psi_j}(\mathbf{x}_t; \emptyset, t)}{w} - \frac{\epsilon}{w}]$  to replace traditional random noise  $\epsilon$ , thereby alleviating the impact of out-of-distribution [89].

**Flow loss:** Flow loss is a commonly used regularization term for dynamic 3DGS. Using the output of the pre-trained 2D optical flow estimation model as ground truth, it can render predicted flow by calculating the displacement of Gaussian primitives over a unit time and splatting these 3D displacements onto a 2D plane [104], [114], [115]. However, this approach has a significant gap, primarily because optical flow is a 2D plane attribute and is susceptible to noise. Selecting Gaussian primitives with correct depth in space and introducing uncertainty through KL divergence to constrain optical flow is a potentially feasible method [106].

**Other loss:** There are also some 2D regularization terms worth discussing. For example, constraining the differences in amplitude and phase between the rendered image and the ground truth in the frequency domain can serve as a loss function to aid training, thereby alleviating overfitting issues [33]. Introducing pseudo-labels for hypothetical viewpoints through noise perturbation can assist training in sparse-view settings [54]. In large-scale scene mapping, constraining the changes in attributes before and after optimization can prevent catastrophic forgetting on 3DGS [129]. Additionally, bundle adjustment is usually an important constraint in pose estimation problems [118], [119], [130].

It should be noted that, whether 2D or 3D regularization is used, overall optimization is sometimes suboptimal due to the large number of primitives in 3DGS. Some primitives often have an uncontrollable impact on the results. Therefore, it is necessary to guide the optimization by selecting important Gaussian primitives using methods such as visibility [120], [122], [131], [134].

**Discussion:** For a specific task, various constraints can often be introduced, including 2D and 3D regularization terms, where many regularization terms are plug-and-play and can directly enhance performance.

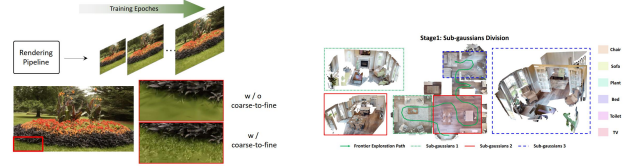
## 6.5 Training Strategy

Training strategy is also an important topic. In this section, we divide it into multi-stage training strategy and end-to-end training strategy, which can be applied to different tasks.

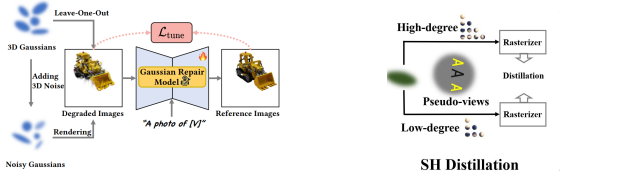
### 6.5.1 Multi-stage Training Strategy

Multi-stage training strategy is a common training paradigm, often involving coarse-to-fine reconstruction. It is widely used for under-determined tasks, such as in AIGC, dynamic 3DGS construction, and SLAM.

Using different 3D representations in different training stages is one of the typical paradigms of multi-stage training. 3DGS→Mesh (training 3DGS in the first stage, converting the representation to Mesh, and then optimizing the Mesh in the second stage) [75], [76], [77], [92], [163], [196] is an effective method to ensure geometric consistency in the generated 3D model. Additionally, instead of converting between 3D representations, generating multi-view images [91], [96], [109], [136], [165], [166], [196] in the first stage to aid



(a) Progressive Optimization [39]. (b) Block Optimization [134].



(c) Robust Optimization [57]. (d) Distillation Strategy [24].

Fig. 9: Four typical End-to-End Training Strategies.

reconstruction in the second stage can also enhance the generation quality.

Two-stage reconstruction for static and dynamic reconstruction is also important in dynamic 3DGS. This type of work typically involves training a time-independent static 3DGS in the first stage, and then training a time-dependent deformation field in the second stage to characterize dynamic Gaussians [115], [143], [144], [145], [146], [168]. Additionally, incremental reconstruction of dynamic scenes frame by frame is also a focus in some works, often relying on the performance of previous reconstructions [135], [140].

In multi-objective optimization tasks, multi-stage training paradigms can enhance training stability and performance. For example, the *coarse-to-fine camera tracking strategy* is a common approach that first obtains a coarse camera pose through a sparse set of pixels, and then further refines the estimated camera pose based on the optimized rendering results [118], [133].

Additionally, some works aim to refine the 3DGS trained in the first stage [51], [57], [80], [87], [170], [179], [188] or endow them with additional capacities, such as semantics [134], [180] and stylization [172]. There are many such training strategies, which are also effective means to maintain training stability and avoid local optima [24]. Furthermore, iterative optimization of the final result to enhance performance is also feasible [136].

### 6.5.2 End-to-End Training Strategy

End-to-end training strategies are often more efficient and can be applied to a wider range of downstream tasks. Some typical works are described in Fig. 9.

**Progressive Optimization Strategy:** This is a commonly used strategy that helps 3DGS prioritize learning global representations before locally optimizing details. In the frequency domain, this process can also be viewed as a progressive learning from low-frequency to high-frequency components. It is often implemented by gradually increasing the proportion of high-frequency signals [33], [187] or introducing progressively larger image/feature sizes for supervision [17], [39], [119], which can also improve efficiency [116]. In generative tasks, progressively selecting the camera pose is also an easy-to-difficult training strategy,

gradually optimizing from positions close to the initial viewpoint to those further away [77], [102].

**Block Optimization Strategy:** This strategy is often used in large-scale scene reconstruction, which can not only improve efficiency but also alleviate the problem of catastrophic forgetting [121], [133], [134]. Similarly, it can achieve reconstruction by partitioning the scene into static backgrounds and dynamic objects [112], [113], [114], [144]. Additionally, such an approach is also applied in AIGC and Semantic Understanding, where refining the reconstruction quality of submaps enhances overall performance [87], [181].

Unlike submaps divided by spatial regions, Gaussian primitives can be categorized into different generations along with their densification process, allowing for the application of different regularization strategies to each generation, which is an effective strategy to regulate the fluidity of different generations [162]. Categorizing the initial points into those on smooth surfaces and independent points is also a feasible strategy. By designing distinct initialization and densification strategies for each category, it can achieve better geometric representation [192]. Additionally, some works aim to design keyframes (or windows) selection strategies based on inter-frame covisibility or geometric overlap ratio in temporal data and use them for reconstructions [118], [120], [122], [126], [129], [141].

**Robust Optimization Strategy:** Introducing noise perturbations during training is a common method to enhance the robustness of the training process [57], [92], [143]. Such perturbations can target camera poses, timestep, and images, and can be regarded as a form of data augmentation to prevent overfitting. Additionally, some training strategies aim to mitigate overfitting and catastrophic forgetting by avoiding continuous training from a single viewpoint [121], [127].

**Distillation-based Strategy:** To compress model parameters, some distillation strategies use the original 3DGS as the teacher model and low-dimensional SH 3DGS as the student model. By introducing more pseudo views, they aim to improve the representational performance of the low-dimensional SH [24].

**Discussion:** Improving training strategies is an efficient way to optimize the training process of 3DGS and can enhance performance in many tasks. End-to-end training strategies, in particular, can improve performance while ensuring efficiency.

## 6.6 Adaptive Control

Adaptive Control of 3DGS is an important process for regulating the number of Gaussian primitives, including cloning, splitting, and pruning. In the following sections, we will summarize existing techniques from the perspectives of densification (cloning and splitting) and pruning.

### 6.6.1 Densification

Densification is crucial, especially for detail reconstruction. In this section, we will analyze it from the perspectives of "Where to densify" and "How to densify". Additionally, we will discuss how to avoid excessive densification.

**Where to Densification:** Densification techniques typically concentrate on identifying positions requiring densification, with this process being governed by gradients in the

original 3DGS, which can also be extended to the reconstruction of new targets in dynamic scenes [140]. Subsequently, the regions with low opacity or silhouette and high depth rendered error, regarded as unreliable areas, have also been considered important factors for guiding densification [32], [118], [129], [134], [148], [160], which are typically used to fill holes or improve regions with 3D inconsistencies. Some works continue to focus on improvements based on gradients, where the number of pixels covered by each Gaussian in different views is considered as weights to dynamically average the gradients of these views, thereby improving the conditions for point cloud growth [198]. Additionally, the SDF value and neighbor distance are also important criteria, with locations closer to the surface and lower compactness being more prone to densification [80], [156], [159].

**How to Densification:** Numerous works have improved densification methods. Graph structures are utilized to explore relationships between nodes and define new Gaussians at the center of edges based on a proximity score, thereby mitigating the impact of sparse viewpoints [54]. To prevent excessive growth in the number of Gaussians, the Candidate Pool Strategy is designed to store pruned Gaussians for densification [94]. Additionally, work [199] introduces three conservation rules to ensure visual consistency and employs integral tensor equations to model densification.

Excessive densification is also unnecessary, as it directly impacts the efficiency of 3DGS. In cases where two Gaussian functions are in close proximity, limiting their densification is a straightforward idea, where the distance between Gaussians can be measured by Gaussian Divergent Significance [96] (GDS) or Kullback–Leibler divergence [62], where  $\mu_1, \Sigma_1, \mu_2, \Sigma_2$  belongs to two adjacent Gaussians.

$$\begin{aligned} \text{GDS} &: \|\mu_1 - \mu_2\|^2 + \text{tr}\left(\Sigma_1 + \Sigma_2 - 2(\Sigma_1^{-1}\Sigma_2\Sigma_1^{-1})^{1/2}\right), \\ \text{KL} &: \frac{1}{2}\left(\text{tr}(\Sigma_2^{-1}\Sigma_1) + \ln\frac{\det\Sigma_1}{\det\Sigma_2} + (\mu_2 - \mu_1)^T\Sigma_2^{-1}(\mu_2 - \mu_1) - 3\right). \end{aligned} \quad (10)$$

And DeblurGS [42] incorporates a Gaussian Densification Annealing strategy to prevent the densification of inaccurate Gaussians during the early training stages at imprecise camera motion estimation. Furthermore, in some downstream tasks, densification is sometimes abandoned to prevent 3DGS from overfitting to each image, which could lead to incorrect geometric shapes [116], [118], [120], [126].

### 6.6.2 Pruning

Removing unimportant Gaussian primitives can ensure efficient representation. In the initial 3DGS framework, opacity was employed as the criterion for determining the significance of a Gaussian. Subsequent research has explored the incorporation of scale as a guiding factor for pruning [74]. However, these approaches primarily focus on individual Gaussian primitives, lacking a comprehensive consideration of the global representation. Therefore, subsequent derivative techniques have addressed this issue.

**Importance scores:** The volume and the hit count on training views can be introduced along with opacity to

jointly determine the global significance score of a Gaussian primitive [24].

$$GS_j = \sum_{i=1}^{MHW} \mathbf{1}(G(\mathbf{X}_j), r_i) \cdot \sigma_j \cdot \gamma(\Sigma_j), \quad (11)$$

where  $\gamma(\Sigma_j)$  and  $\mathbf{1}(G(\mathbf{X}_j), r_i)$  are volume and the hit count, and  $M$  represent the number of training views. Subsequently, Gaussians are ranked according to their global significance scores, and the ones with the lowest scores are pruned. Similar importance scores were improved in other works [200], [201].

**Multi-view consistency:** Multi-view consistency is a key criterion for determining whether Gaussians need to be pruned. For example, work [126] prunes newly added Gaussians that are not observed by three keyframes within a local keyframe window, while work [131] prunes Gaussians that are invisible in all virtual views but visible in real views.

**Distance Metric:** Some surface-aware methods often introduce the distance to the surface [118] and SDF values [159], pruning Gaussian primitives that are far from the surface. The distance between Gaussians is also an important metric. GauHuman [62] aims to "merge" Gaussians with small scaling and low KL divergence, as mentioned in Eq. 10.

**Learnable control parameter:** Introducing a learnable mask based on scale and opacity to determine whether target Gaussian primitives should be removed is also an effective way to prevent 3DGS from becoming overly dense [23].

## 6.7 Post-Processing

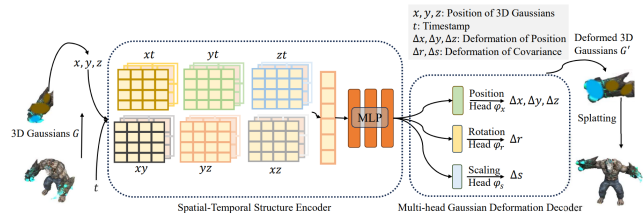
Post-processing strategies for pre-trained Gaussians are important, as they can improve the original efficiency and performance of 3DGS. Common post-processing often improves Gaussian representations through different optimization strategies. This type of work has been discussed in Sec. 6.5.

**Representation Conversion:** Pre-trained 3DGS can be directly converted to Mesh by introducing Poisson reconstruction [202] on sampled 3D points [156], [160]. Similarly, Gaussian Opacity Fields (GOF) [161] introduces 3D bounding boxes to convert pre-trained 3DGS to a Tetrahedral Grid representation, and then it extracts triangle meshes from it using Binary Search of Level Set. Additionally, LGM [92] first converts pre-trained 3DGS to NeRF representation, and then uses NeRF2Mesh [203] to convert it to Mesh.

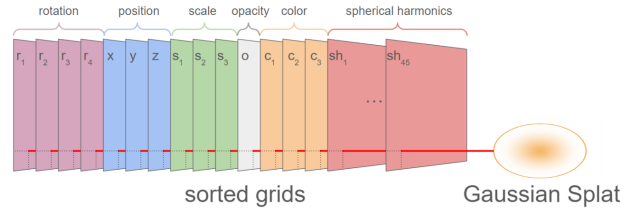
**Performance and Efficiency:** Some works aim to enhance the performance of 3DGS in certain tasks through post-processing, such as multi-scale rendering. Based on pretrained 3DGS, SA-GS [36] introduces a 2D scale-adaptive filter that dynamically adjusts scales based on testing frequency to enhance anti-aliasing performance when zooming out. In terms of efficiency, removing redundant Gaussian primitives from pre-trained 3DGS [29] or introducing a Gaussians caching mechanism [204] can effectively improve rendering efficiency.

## 6.8 Integration with Other Representations

The convertible nature of 3D representations facilitates the integration of 3DGS with other representations. Such works often leverage the advantages of other representations to improve the original 3DGS.



(a) Extending Triplane to 4D Space [145].



(b) Mapping 3D Gaussian onto a 2D Grid [25].

Fig. 10: Two auxiliary representations of 3DGS.

### 6.8.1 Point Clouds

Point clouds, as a 3D representation related to 3DGS, are often used to initialize its attributes. Converting point cloud representations to 3DGS can effectively fill in the point clouds' holes [100], [102], which is typically done after high-precision reconstruction of the point clouds. Conversely, 3DGS can also be converted into point clouds, followed by voxelizing the point cloud into 3D voxels and then projecting them onto 2D BEV grids, which is an important guide in navigation tasks [134].

Additionally, anchor points in space can assist 3DGS. These methods use the centers of voxels as anchor points to represent the scene. Each anchor point comprises a local context feature, a scaling factor, and multiple learnable offsets. By decoding other attributes based on these offsets and features, the anchors are transformed into local neural Gaussians. This idea helps mitigate the redundant expansion of 3DGS [26], [39], [159].

### 6.8.2 Mesh

Meshes have better geometric representation capabilities and can, to some extent, alleviate artifacts or blurry pixels caused by 3DGS [142]. They are still the most widely used 3D representation in downstream tasks [92].

A considerable amount of work has discussed how to convert 3DGS to Mesh, as mentioned in Sec. 5.2. Once converted, they can be further optimized to achieve better geometric and appearance [64], [75], [76], [163].

Jointly optimizing 3DGS and Mesh is also an optional strategy. 3DGS is suitable for constructing complex geometric structures, while Mesh can be used to reconstruct detailed color appearances on smooth surfaces. Combining the two can enhance reconstruction performance [142].

### 6.8.3 Triplane

Triplane is notable for its compactness and efficient expressiveness [50], which can be considered an encoded

representation. Thanks to these characteristics, triplane is often used in generalization-related tasks. Specifically, a triplane consists of three orthogonal feature planes: the  $X$ - $Y$  plane, the  $Y$ - $Z$  plane, and the  $X$ - $Z$  plane. Features can be obtained by accessing positions in the space, and these features are subsequently decoded to predict Gaussian attributes [50], [51], [60], [93].

Subsequent works [107], [145], [168] attempt to extend the triplane to 4D space ( $XYZT$ ) by introducing multi-scale HexPlanes [108] or 4D GaussianPlanes [168] to enhance the continuity of 4DGS in the spatiotemporal dimension, as shown in Fig. 10(a).

#### 6.8.4 Grid

Grid is also an efficient representation, as it can access grid corners and interpolate to obtain features or attributes at specific positions. Hash grid [9], as one of the representative methods, has the ability to compress scenes and obtain a more compact and efficient 3DGS [23], [63], [116], [172], [182]. Furthermore, Self-Organizing Gaussian [25] maps the original unstructured 3D Gaussian onto a 2D grid to preserve local spatial relationships, where adjacent Gaussians will have similar attribute values, thereby reducing the memory storage of the scene and maintaining continuity in 3D space, as shown in Fig. 10(b).

#### 6.8.5 Implicit Representation

Implicit representations, benefiting from their representation capability, can be used to mitigate the condition difficulty and surface artifacts of 3DGS [72]. Specifically, introducing NeRF to encode color and opacity can significantly enhance the representation’s adjustability [205]. Moreover, by designing an SDF-to-opacity transformation function [158] or employing mutual geometry supervision [159] to jointly optimize 3DGS and SDF representations, the surface reconstruction performance of 3DGS can be improved.

#### 6.8.6 GaussianVolumes

GaussianVolumes are also utilized for generalizable representations [94], where a volume is composed of a fixed number of 3DGS. This representation maintains the efficiency of Gaussian representations while offering greater manipulability compared to the generalized triplane representation and alleviating the dependence on the accuracy of point cloud predictions.

**Discussion:** Depending on different needs, various representations can be introduced. However, efficiently converting between different representations is important.

### 6.9 Guidance by Additional Prior

When dealing with under-determined problems, such as sparse view settings 3.3.1, introducing additional priors is a straightforward method to improve 3DGS performance.

**Pre-trained Models:** Introducing pre-trained models is an effective paradigm that can guide the optimization through the model’s knowledge. Pre-trained monocular depth models and point cloud prediction models are a common type of prior, where the predicted depth values and positions can be used for the initialization and regularization [52], [54], [55], [100], [102], [131]. Pre-trained 2D image (or 3D and

video) generative models are also important in some AIGC-related tasks. They can be used not only for optimization in combination with SDS Loss [80], [103], [196] but also for directly generating (or editing) images for training [91], [100], [102], [109]. Similarly, some works introduce pre-trained image inpainting networks to alleviate difficulties caused by occlusion as well as overlap [77], [100], [102], [162], [171] or super-resolution models for a high level of detail [102], [168] during the generation process. Additionally, pre-trained ControlNet [167] or Large Language Models can also be used to guide 3D generation. The former can enhance geometric consistency under depth guidance [77], [78], [166], while the latter can predict layout maps to guide spatial relationships in multi-object 3D generation scenarios [78]. Notably, certain pre-trained models can endow 3DGS with additional capabilities, such as semantic understanding models, as discussed in Sec. 5.4 and spatial understanding models [131].

**More Sensors:** Due to the 3D-agnostic nature of 2D images, reconstructing 3DGS can be challenging, especially in large-scale reconstructions such as SLAM and autonomous driving. Therefore, incorporating additional sensors for 3D depth information, including depth sensors [121], [127], [129], [130], [131], LiDAR [112], [116], [133], and optical tactile sensors [55], has the potential to alleviate this issue.

**Task-specific Priors:** Some reconstruction tasks, such as human reconstruction, target subjects with certain common characteristics. These characteristics, such as template models and Linear Blend Skinning, can be extracted as priors to guide the reconstruction of similar targets. In the reconstruction, animation, and generation of non-rigid objects, many works utilize SMPL [66] and SMAL [206] to provide strong priors for representing the motion and deformation of non-rigid objects like humans [58], [60], [62], [63], [74] and animals [111], [189]. Subsequently, based on the SMPL template, Shell Maps [95] and template meshes are also introduced in combination with 3DGS to address issues of low efficiency in 3DGAN [73] and unclear geometry [64], [65]. Similarly, in head and face reconstruction and animation tasks, some works [68], [70] also use the FLAME model [69] as a prior. Linear Blend Skinning [151] is also employed as prior knowledge to assist in the prediction of 3DGS motion [70], [150]. Additionally, in 3D urban scene reconstruction tasks, HUGS [114] introduces the Unicycle Model to model the motion of dynamic vehicles, thereby making the motion modeling of moving objects smoother.

## 7 INTERRELATIONSHIPS AND CHALLENGES

As previously mentioned in Sec.3, Sec.4, and Sec.5, there is a substantial amount of research focused on the optimization, application, and extension of 3DGS. However, these discussions often overcomplicate the issue. In this section, we aim to summarize the commonalities across different tasks and propose four core challenges along with their corresponding technical discussions, as shown in Tab.2. Recognizing these common challenges and solutions can simplify research efforts and promote interdisciplinary progress.

TABLE 2: The Relationships among Challenges, Tasks, and Technological Improvement.

Challenges	Major Tasks	Major Technological Improvements
<i>Suboptimal Data Challenges 7.1</i>	<b>Limited Number:</b> Sparse Views 3.3.2, Autonomous Driving Reconstruction 4.3.1, Dynamic 3DGS 5.1 (Monocular Video Part 5.1.2), AIGC 4.2 and Editable 3DGS 5.3. <b>Limited Quality:</b> Slam 4.3.2 and Reconstruction under blurred images (Sec.3.2) or without poses [207], [208]	<b>Limited Number:</b> Initialization 6.1, Regularization 6.4, Adaptive Control 6.6 Training Strategies 6.5, and Guidance by Additional Prior 6.9. <b>Limited Quality:</b> Training Strategies 6.5 and Integration with Other Representations (Sec. 6.8)
<i>Generalization Challenges 7.2</i>	Generalization 3.3.1, and Generalization-related tasks in the Human Reconstruction 4.1 and AIGC 4.2	Initialization 6.1, Adaptive Control 6.6, and Integration with Other Representations 6.8
<i>Physics Challenges 7.3</i>	<b>Physical Motion:</b> Dynamic 3DGS 5.1, Physics Simulation 5.5, Animation 5.3.4, Dynamic Human 4.1 and Autonomous Driving Reconstruction 4.3.1. <b>Physical Rendering:</b> Photorealism 3.2 and Physics Simulation 5.5.	<b>Physical Motion and Rendering:</b> Attribute Expansion 6.2, Regularization Strategy 6.4, and Guidance by Additional Prior 6.9.
<i>Realness and Efficiency Challenges 7.4</i>	<b>Realness:</b> Photorealism 3.2, Surface Reconstruction 5.2, Semantic Understanding 5.4, some AIGC-related 4.2 and Autonomous Driving 4.3 works. <b>Efficiency:</b> Efficiency 3.1, some works in Autonomous Driving 4.3 and Semantic Understanding 5.4	<b>Realness:</b> Most of the technologies in 6. <b>Efficiency:</b> Attribute Expansion 6.2, Post-Processing 6.7, Adaptive Control 6.6 and Splatting 6.3.

### 7.1 Suboptimal Data Challenges

In real-world scenarios, collecting a large volume of high-quality training data is often impractical. On one hand, without access to 3D data and sufficient multi-view images, relying solely on a limited number of 2D image supervisions is insufficient for accurate 3DGS reconstruction. For instance, with only a frontal image of a target, inferring the appearance of the back is highly challenging. On the other hand, data quality is equally critical; accurate poses and clear images directly influence reconstruction performance.

Such problems are discussed across multiple tasks, such as Sparse Views Setting (Sec.3.3.1), Autonomous Driving (Sec.4.3), Dynamic 3DGS (Sec.5.1) (Monocular Video), AIGC (Sec.4.2), and Editable 3DGS (Sec.5.3). Numerous works have discussed how to improve initialization (Sec.6.1), regularization (Sec.6.4), adaptive control (Sec.6.6), and training strategies (Sec.6.5), or introduce additional priors (Sec.6.9) in the context of sparse or missing multi-view training images. Additionally, reconstruction with missing accurate poses can also be considered an underdetermined problem. This is discussed in the SLAM literature (Sec.4.3.2) and reconstruction under blurred images (Sec.3.2) or without poses [207], [208], where new training strategies (Sec. 6.5) and other representations (Sec. 6.8) are often introduced to mitigate it.

### 7.2 Generalization Challenges

Despite the improved training efficiency compared to NeRF, the scene-specific training paradigm remains a major bottleneck for the application of 3DGS. It is hard to imagine having to train for each target or scene individually, especially in multi-target reconstruction and text-to-scene generation.

We find that this issue is commonly discussed in the Generalization setting (Sec.3.3.1) and in some Generalization-related tasks in Human Reconstruction (Sec.4.1) and AIGC (Sec.4.2). These works aim to directly infer new scenes using feedforward networks. Therefore, they exhibit strong technical similarities, such as the introduction of triplanes. Specific improvement strategies are extensively analyzed

in initialization (Sec.6.1), adaptive control (Sec.6.6), and integration with other representations (Sec.6.8).

### 7.3 Physics Challenges

Traditional 3DGS only considers static rendering and neglects the laws of physics motion, which are important in simulations [139]. Additionally, physically-based rendering is a significant step towards applying 3DGS to simulate the physical world. Thanks to the explicit representation, it is possible to construct 3DGS that adhere to physical laws.

This issue is commonly discussed in Dynamic 3DGS (Sec.5.1), Physics Simulation (Sec.5.5), Animation (Sec.5.3.4), and some dynamic Human Reconstruction (Sec.4.1) or Autonomous Driving Scene Reconstruction (Sec.4.3.1). These discussions focus on how Gaussian primitives should move in the physical world, and physically-based rendering is introduced in Photorealism (Sec.3.2). From a technical perspective, since the early stages of 3DGS research, numerous works have addressed this issue, often focusing on attribute expansion (Sec.6.2), regularization strategy (Sec.6.4), and the assistance of additional priors (Sec. 6.9).

### 7.4 Realness and Efficiency Challenges

Realness and efficiency challenges are fundamental issues. They are investigated in various works and have been discussed in Sec. 3. In this section, we discuss some typical related tasks and summarize their common techniques.

Regarding the Realness challenges, existing works have discussed not only Photorealism (Sec.3.2), Surface Reconstruction (Sec.5.2), and Semantic Understanding (Sec.5.4), but also addressed this issue in AIGC-related (Sec.4.2) and Autonomous Driving (Sec.4.3) research. Most of the techniques mentioned in (Sec.6) contribute to the improvement of rendering performance. Different methods are employed for different tasks. For instance, AIGC-related works (Sec.4.2) often focus on improving training strategies (Sec.6.5) and regularization (Sec.6.4), while Surface Reconstruction works (Sec.5.2) are related to post-processing procedures (Sec. 6.7).

Regarding the efficiency challenges (Sec.3.1), they are mentioned in some derivative tasks, such as those related to

Autonomous Driving (Sec.4.3) and Semantic Understanding (Sec.5.4). Existing improvements often focus on introducing additional attributes (Sec.6.2) or post-processing (Sec.6.7), as well as improving adaptive control (Sec.6.6) and splatting (Sec. 6.3) strategies.

In addition, there are some relationships between different domains that have not been mentioned. For instance, Surface Reconstruction techniques (Sec.5.2) are often referenced in the context of Editable 3DGS (Sec.5.3), etc.

## 8 OPPORTUNITIES

3DGS has recently experienced significant development, with numerous works demonstrating its potential in related tasks. In this section, we discuss unresolved issues among the aforementioned core challenges and propose potential directions for future studies. Additionally, we discuss some extensions of applications and technologies.

### 8.1 Suboptimal Training Data

An ideal 3DGS training process necessitates sufficient and high-quality data, but in practical applications, this is often excessively challenging. Although focusing on the introduction of priors can mitigate the problem to some extent, optimizing a large number of Gaussians under underconstrained conditions remains inherently difficult. Therefore, a potential solution is to reduce the number of Gaussian primitives based on their uncertainty while enhancing the representational capacity of individual primitives [27]. This involves finding a trade-off between the number of Gaussians and rendering performance, thereby improving the efficiency of utilizing sparse samples.

Then, poor-quality data should also be taken into consideration. Unconstrained in-the-wild images are a typical case, encompassing transient occlusions and dynamic appearance changes, such as varying sky, weather, and lighting, which have been extensively discussed in NeRF [209], [210], [211]. To enhance efficiency, existing works have also discussed this issue in the context of 3DGS [212], [213], which attempt to model appearance changes and handle transient objects. However, their performance struggles, especially in scenes with complex lighting changes and frequent occlusions. Thanks to the explicit representation characteristics of 3DGS, decoupling geometric representations and introducing geometric consistency constraints across different scenes is a promising approach to mitigate instability during the training process.

### 8.2 Generalization

Although existing generalization-related works can directly obtain scene representations through forward inference, their performance is often unsatisfactory and limited by the type of scene [46], [49], [50], [93]. We hypothesize that this is due to the difficulty of feedforward networks in performing adaptive control of 3DGS, as also mentioned in [47]. In future research, designing a reference-feature-based feedforward adaptive control strategy is a potential solution, which can predict the positions requiring adaptive control through reference features and be plug-and-play into existing generalization-related works. Additionally, existing

generalization-related works rely on accurate poses, which are often difficult to obtain in practical applications [208], [214], [215]. Therefore, discussing generalizable 3DGS under pose-missing conditions is also promising [204].

## 8.3 Physics Problems

### 8.3.1 Physically-based Motion

Ensuring that the motion of 3DGS adheres to physical laws is essential for unifying simulation and rendering [139]. Although rigidity-related regularization terms have been introduced, as described in Sec.6.4.1, most existing works focus on animating 3DGS while neglecting the physical attributes of the Gaussian primitives themselves (Sec.5.1). Some pioneering works attempt to introduce velocity attributes [106] and Newtonian dynamics rules [139], but this is not sufficient to fully describe the physical motion of 3DGS in space. A potential solution is to introduce more physical attributes in Gaussian primitives, such as material [216], acceleration, and force distribution, which can be constrained by priors from certain simulation tools and physics knowledge.

### 8.3.2 physically-based rendering

Physically-based rendering is also a direction worth attention, as it enables 3DGS to handle relighting and material editing, producing outstanding inverse rendering results [40]. Future works can explore decoupling geometry and appearance in 3DGS, conducting research from the perspectives of normal reconstruction and the modeling of illumination and materials [72], [216], [217].

## 8.4 Realness and Efficiency

### 8.4.1 Surface Reconstruction

The difficulty in reconstructing clear surfaces has always been a significant challenge affecting rendering realism. As discussed in Sec. 5.2, some works have addressed this issue, attempting to represent surfaces with planar Gaussians. However, this can result in a decline in rendering performance, possibly due to the reduced representational capacity of planar Gaussian primitives or the instability of the training process. Therefore, designing Gaussian primitives that are better suited for surface representation and introducing a multi-stage training paradigm along with regularization terms are potential solutions.

### 8.4.2 Efficiency

Storage efficiency is one of the critical bottlenecks of 3DGS. Existing works focus on introducing VQ techniques and compressing SH parameters, as discussed in Sec. 3.1.1. However, such approaches inevitably affect rendering performance. Therefore, exploring how to design more efficient representations based on 3DGS is a potential way to enhance efficiency [26], [27], while maintaining performance.

## 8.5 Application

### 8.5.1 Large-scale Gaussian Splatting

Although recent methods are capable of efficient reconstruction in small-scale and object-centric scenes, extending this

capability to large-scale scenes remains challenging due to limited video memory, lengthy optimization times, and significant appearance changes. Some recent works have attempted to address these issues. For example, VastGaussian [218] intuitively uses a region division mechanism based on camera positions to divide large scenes into multiple small blocks and introduces additional auxiliary camera positions based on a spatially-aware visibility criterion, thus achieving precise reconstruction for each small region. Similarly, Fed3DGS [219] introduces a federated learning framework into large-scale 3DGS to reduce the data load on the central server and implements a Gaussian merging strategy, enabling decentralized reconstruction among millions of clients and distributed computing resources. Following these approaches, there remains substantial research space.

### 8.5.2 AIGC

Existing AIGC-related works mostly focus on the generation of single static objects. However, in practical applications, the generation of multiple objects (Sec.4.2.3) and dynamic objects (Sec.4.2.4) are more important. Additionally, in constructing scenes with multiple moving objects, characterizing the objects interactions is also a worthwhile research task.

### 8.5.3 Application Expansion

Thanks to the efficient and robust reconstruction capabilities of 3DGS, numerous applications have garnered attention in various fields, such as medicine [220], industrial defect detection [221], image compression [222], and aviation [223]. In the future, 3DGS could potentially replace NeRF for 3D reconstruction in additional fields, such as robotics [224] and biology [225].

## 8.6 Technical Improvements

### 8.6.1 Initialization

An increasing number of research and engineering projects have found that initialization is important in 3DGS. Traditional SfM initialization is not suitable for many constrained scenarios, such as sparse view settings, AIGC, and low-light reconstruction. Therefore, more robust initialization methods should be designed to replace random initialization in these constrained scenarios.

### 8.6.2 Splatting

Splatting also plays an important role in 3DGS, but it is rarely mentioned in existing works [190], [191]. Designing efficient parallel splatting strategies on pretrained 3DGS has the potential to impact rendering performance and efficiency.

## 9 CONCLUSION

The burgeoning interest in the field of 3D Gaussian Splatting (3DGS) has precipitated the emergence of a myriad of related downstream tasks and technologies, thereby contributing to an increasing complexity and confusion within the domain, which manifest in various forms, including the similar motivations across different works; the incorporation of similar technologies across disparate tasks; and the nuanced differences and interconnections between various technologies. In this survey, we endeavor to systematically categorize

existing works based on their underlying motivations and critically discuss the associated technologies. Our objective is to elucidate common challenges across different tasks and technologies, thereby providing a coherent framework for comprehending this rapidly evolving field. This survey aspires to serve as an invaluable resource for both newcomers and seasoned practitioners, facilitating navigation and effective engagement with recent advancements. Additionally, we identify and highlight prospective avenues for future research, aiming to inspire continued innovation and exploration in 3DGS.

## REFERENCES

- [1] G. Chen and W. Wang, "A survey on 3d gaussian splatting," *arXiv preprint arXiv:2401.03890*, 2024.
- [2] T. Wu, Y.-J. Yuan, L.-X. Zhang, J. Yang, Y.-P. Cao, L.-Q. Yan, and L. Gao, "Recent advances in 3d gaussian splatting," *Computational Visual Media*, pp. 1–30, 2024.
- [3] B. Fei, J. Xu, R. Zhang, Q. Zhou, W. Yang, and Y. He, "3d gaussian splatting as new era: A survey," *IEEE Transactions on Visualization and Computer Graphics*, 2024.
- [4] K. Gao, Y. Gao, H. He, D. Lu, L. Xu, and J. Li, "Nerf: Neural radiance field in 3d vision, a comprehensive review," *arXiv preprint arXiv:2210.00379*, 2022.
- [5] P. Z. Ramirez, L. De Luigi, D. Sirocchi, A. Cardace, R. Spezialetti, F. Ballerini, S. Salti, and L. Di Stefano, "Deep learning on object-centric 3d neural fields," *IEEE Transactions on Pattern Analysis and Machine Intelligence*, 2024.
- [6] G. Wu, Y. Liu, L. Fang, and T. Chai, "Revisiting light field rendering with deep anti-aliasing neural network," *IEEE Transactions on Pattern Analysis and Machine Intelligence*, vol. 44, no. 9, pp. 5430–5444, 2021.
- [7] B. Mildenhall, P. P. Srinivasan, M. Tancik, J. T. Barron, R. Ramamoorthi, and R. Ng, "Nerf: Representing scenes as neural radiance fields for view synthesis," *Communications of the ACM*, vol. 65, no. 1, pp. 99–106, 2021.
- [8] J. T. Barron, B. Mildenhall, D. Verbin, P. P. Srinivasan, and P. Hedman, "Mip-nerf 360: Unbounded anti-aliased neural radiance fields," in *Proceedings of the IEEE/CVF Conference on Computer Vision and Pattern Recognition*, 2022, pp. 5470–5479.
- [9] T. Müller, A. Evans, C. Schied, and A. Keller, "Instant neural graphics primitives with a multiresolution hash encoding," *ACM transactions on graphics (TOG)*, vol. 41, no. 4, pp. 1–15, 2022.
- [10] C. Sun, M. Sun, and H.-T. Chen, "Direct voxel grid optimization: Super-fast convergence for radiance fields reconstruction," in *Proceedings of the IEEE/CVF Conference on Computer Vision and Pattern Recognition*, 2022, pp. 5459–5469.
- [11] A. Chen, Z. Xu, A. Geiger, J. Yu, and H. Su, "Tensorf: Tensorial radiance fields," in *European Conference on Computer Vision*. Springer, 2022, pp. 333–350.
- [12] D. Rückert, L. Franke, and M. Stamminger, "Adop: Approximate differentiable one-pixel point rendering," *ACM Transactions on Graphics (ToG)*, vol. 41, no. 4, pp. 1–14, 2022.
- [13] K.-A. Aliev, A. Sevastopolsky, M. Kolos, D. Ulyanov, and V. Lempitsky, "Neural point-based graphics," in *Computer Vision—ECCV 2020: 16th European Conference, Glasgow, UK, August 23–28, 2020, Proceedings, Part XXII 16*. Springer, 2020, pp. 696–712.
- [14] O. Wiles, G. Gkioxari, R. Szeliski, and J. Johnson, "Synsin: End-to-end view synthesis from a single image," in *Proceedings of the IEEE/CVF conference on computer vision and pattern recognition*, 2020, pp. 7467–7477.
- [15] B. Kerbl, G. Kopanas, T. Leimkühler, and G. Drettakis, "3d gaussian splatting for real-time radiance field rendering," *ACM Transactions on Graphics*, vol. 42, no. 4, pp. 1–14, 2023.
- [16] M. Zwicker, H. Pfister, J. Van Baar, and M. Gross, "Ewa volume splatting," in *Proceedings Visualization, 2001. VIS'01*. IEEE, 2001, pp. 29–538.
- [17] S. Girish, K. Gupta, and A. Shrivastava, "Eagles: Efficient accelerated 3d gaussians with lightweight encodings," *arXiv preprint arXiv:2312.04564*, 2023.
- [18] K. Navaneet, K. P. Meibodi, S. A. Koohpayegani, and H. Pirsiavash, "Compact3d: Compressing gaussian splat radiance field models with vector quantization," *arXiv preprint arXiv:2311.18159*, 2023.



- [19] S. Niedermayr, J. Stumpfegger, and R. Westermann, "Compressed 3d gaussian splatting for accelerated novel view synthesis," *arXiv preprint arXiv:2401.02436*, 2023.
- [20] W. H. Equitz, "A new vector quantization clustering algorithm," *IEEE transactions on acoustics, speech, and signal processing*, vol. 37, no. 10, pp. 1568–1575, 1989.
- [21] D. Sculley, "Web-scale k-means clustering," in *Proceedings of the 19th international conference on World wide web*, 2010, pp. 1177–1178.
- [22] P. Deutsch, "Deflate compressed data format specification version 1.3," Tech. Rep., 1996.
- [23] J. C. Lee, D. Rho, X. Sun, J. H. Ko, and E. Park, "Compact 3d gaussian representation for radiance field," *arXiv preprint arXiv:2311.13681*, 2023.
- [24] Z. Fan, K. Wang, K. Wen, Z. Zhu, D. Xu, and Z. Wang, "Lightgaussian: Unbounded 3d gaussian compression with 15x reduction and 200+ fps," *arXiv preprint arXiv:2311.17245*, 2023.
- [25] W. Morgenstern, F. Barthel, A. Hilsmann, and P. Eisert, "Compact 3d scene representation via self-organizing gaussian grids," *arXiv preprint arXiv:2312.13299*, 2023.
- [26] T. Lu, M. Yu, L. Xu, Y. Xiangli, L. Wang, D. Lin, and B. Dai, "Scaffold-gs: Structured 3d gaussians for view-adaptive rendering," *arXiv preprint arXiv:2312.00109*, 2023.
- [27] A. Hamdi, L. Melas-Kyriazi, J. Mai, G. Qian, R. Liu, C. Vondrick, B. Ghanem, and A. Vedaldi, "Ges: Generalized exponential splatting for efficient radiance field rendering," in *Proceedings of the IEEE/CVF Conference on Computer Vision and Pattern Recognition*, 2024, pp. 19 812–19 822.
- [28] S. Durvasula, A. Zhao, F. Chen, R. Liang, P. K. Sanjaya, and N. Vijaykumar, "Distwar: Fast differentiable rendering on raster-based rendering pipelines," *arXiv preprint arXiv:2401.05345*, 2023.
- [29] J. Jo, H. Kim, and J. Park, "Identifying unnecessary 3d gaussians using clustering for fast rendering of 3d gaussian splatting," *arXiv preprint arXiv:2402.13827*, 2024.
- [30] J. Lee, S. Lee, J. Lee, J. Park, and J. Sim, "Gscore: Efficient radiance field rendering via architectural support for 3d gaussian splatting," in *Proceedings of the 29th ACM International Conference on Architectural Support for Programming Languages and Operating Systems, Volume 3*, 2024, pp. 497–511.
- [31] D. Verbin, P. Hedman, B. Mildenhall, T. Zickler, J. T. Barron, and P. P. Srinivasan, "Ref-nerf: Structured view-dependent appearance for neural radiance fields," in *2022 IEEE/CVF Conference on Computer Vision and Pattern Recognition (CVPR)*. IEEE, 2022, pp. 5481–5490.
- [32] K. Cheng, X. Long, K. Yang, Y. Yao, W. Yin, Y. Ma, W. Wang, and X. Chen, "Gaussianpro: 3d gaussian splatting with progressive propagation," *arXiv preprint arXiv:2402.14650*, 2024.
- [33] J. Zhang, F. Zhan, M. Xu, S. Lu, and E. Xing, "Fregs: 3d gaussian splatting with progressive frequency regularization," *arXiv preprint arXiv:2403.06908*, 2024.
- [34] Z. Yan, W. F. Low, Y. Chen, and G. H. Lee, "Multi-scale 3d gaussian splatting for anti-aliased rendering," *arXiv preprint arXiv:2311.17089*, 2023.
- [35] Z. Yu, A. Chen, B. Huang, T. Sattler, and A. Geiger, "Mip-splatting: Alias-free 3d gaussian splatting," in *Proceedings of the IEEE/CVF Conference on Computer Vision and Pattern Recognition*, 2024, pp. 19 447–19 456.
- [36] X. Song, J. Zheng, S. Yuan, H.-a. Gao, J. Zhao, X. He, W. Gu, and H. Zhao, "Sa-gs: Scale-adaptive gaussian splatting for training-free anti-aliasing," *arXiv preprint arXiv:2403.19615*, 2024.
- [37] Y. Jiang, J. Tu, Y. Liu, X. Gao, X. Long, W. Wang, and Y. Ma, "Gaussianshader: 3d gaussian splatting with shading functions for reflective surfaces," in *Proceedings of the IEEE/CVF Conference on Computer Vision and Pattern Recognition*, 2024, pp. 5322–5332.
- [38] J. Meng, H. Li, Y. Wu, Q. Gao, S. Yang, J. Zhang, and S. Ma, "Mirror-3dgs: Incorporating mirror reflections into 3d gaussian splatting," *arXiv preprint arXiv:2404.01168*, 2024.
- [39] Z. Yang, X. Gao, Y. Sun, Y. Huang, X. Lyu, W. Zhou, S. Jiao, X. Qi, and X. Jin, "Spec-gaussian: Anisotropic view-dependent appearance for 3d gaussian splatting," *arXiv preprint arXiv:2402.15870*, 2024.
- [40] J. Gao, C. Gu, Y. Lin, H. Zhu, X. Cao, L. Zhang, and Y. Yao, "Relightable 3d gaussian: Real-time point cloud relighting with brdf decomposition and ray tracing," *arXiv preprint arXiv:2311.16043*, 2023.
- [41] B. Walter, S. R. Marschner, H. Li, and K. E. Torrance, "Microfacet models for refraction through rough surfaces," in *Proceedings of the 18th Eurographics conference on Rendering Techniques*, 2007, pp. 195–206.
- [42] J. Oh, J. Chung, D. Lee, and K. M. Lee, "Deblurgs: Gaussian splatting for camera motion blur," *arXiv preprint arXiv:2404.11358*, 2024.
- [43] Y. Bao, T. Ding, J. Huo, W. Li, Y. Li, and Y. Gao, "Insertnerf: Instilling generalizability into nerf with hypernet modules," *arXiv preprint arXiv:2308.13897*, 2023.
- [44] P. Wang, X. Chen, T. Chen, S. Venugopalan, Z. Wang *et al.*, "Is attention all that nerf needs?" *arXiv preprint arXiv:2207.13298*, 2022.
- [45] X. Gao, J. Yang, J. Kim, S. Peng, Z. Liu, and X. Tong, "Mps-nerf: Generalizable 3d human rendering from multiview images," *IEEE Transactions on Pattern Analysis and Machine Intelligence*, 2022.
- [46] S. Szymanowicz, C. Ruppel, and A. Vedaldi, "Splatter image: Ultra-fast single-view 3d reconstruction," *arXiv preprint arXiv:2312.13150*, 2023.
- [47] D. Charatan, S. Li, A. Tagliasacchi, and V. Sitzmann, "pixelsplat: 3d gaussian splats from image pairs for scalable generalizable 3d reconstruction," *arXiv preprint arXiv:2312.12337*, 2023.
- [48] A. Chen, Z. Xu, F. Zhao, X. Zhang, F. Xiang, J. Yu, and H. Su, "Mvsnrnf: Fast generalizable radiance field reconstruction from multi-view stereo," in *Proceedings of the IEEE/CVF international conference on computer vision*, 2021, pp. 14 124–14 133.
- [49] Y. Chen, H. Xu, C. Zheng, B. Zhuang, M. Pollefeys, A. Geiger, T.-J. Cham, and J. Cai, "Mvsplat: Efficient 3d gaussian splatting from sparse multi-view images," *arXiv preprint arXiv:2403.14627*, 2024.
- [50] Z.-X. Zou, Z. Yu, Y.-C. Guo, Y. Li, D. Liang, Y.-P. Cao, and S.-H. Zhang, "Triplane meets gaussian splatting: Fast and generalizable single-view 3d reconstruction with transformers," *arXiv preprint arXiv:2312.09147*, 2023.
- [51] D. Xu, Y. Yuan, M. Mardani, S. Liu, J. Song, Z. Wang, and A. Vahdat, "Agg: Amortized generative 3d gaussians for single image to 3d," *arXiv preprint arXiv:2401.04099*, 2024.
- [52] J. Chung, J. Oh, and K. M. Lee, "Depth-regularized optimization for 3d gaussian splatting in few-shot images," *arXiv preprint arXiv:2311.13398*, 2023.
- [53] J. L. Schonberger and J.-M. Frahm, "Structure-from-motion revisited," in *Proceedings of the IEEE conference on computer vision and pattern recognition*, 2016, pp. 4104–4113.
- [54] Z. Zhu, Z. Fan, Y. Jiang, and Z. Wang, "Fsgs: Real-time few-shot view synthesis using gaussian splatting," *arXiv preprint arXiv:2312.00451*, 2023.
- [55] A. Swann, M. Strong, W. K. Do, G. S. Camps, M. Schwager, and M. Kennedy III, "Touch-gs: Visual-tactile supervised 3d gaussian splatting," *arXiv preprint arXiv:2403.09875*, 2024.
- [56] J. Li, J. Zhang, X. Bai, J. Zheng, X. Ning, J. Zhou, and L. Gu, "Dngaussian: Optimizing sparse-view 3d gaussian radiance fields with global-local depth normalization," *arXiv preprint arXiv:2403.06912*, 2024.
- [57] C. Yang, S. Li, J. Fang, R. Liang, L. Xie, X. Zhang, W. Shen, and Q. Tian, "Gaussianobject: Just taking four images to get a high-quality 3d object with gaussian splatting," *arXiv preprint arXiv:2402.10259*, 2024.
- [58] A. Moreau, J. Song, H. Dharmo, R. Shaw, Y. Zhou, and E. Pérez-Pellitero, "Human gaussian splatting: Real-time rendering of animatable avatars," *arXiv preprint arXiv:2311.17113*, 2023.
- [59] S. Zheng, B. Zhou, R. Shao, B. Liu, S. Zhang, L. Nie, and Y. Liu, "GPS-Gaussian: Generalizable Pixel-wise 3D Gaussian Splatting for Real-time Human Novel View Synthesis," 2024.
- [60] M. Kocabas, J.-H. R. Chang, J. Gabriel, O. Tuzel, and A. Ranjan, "Hugs: Human gaussian splats," *arXiv preprint arXiv:2311.17910*, 2023.
- [61] L. Hu, H. Zhang, Y. Zhang, B. Zhou, B. Liu, S. Zhang, and L. Nie, "Gaussianavatar: Towards realistic human avatar modeling from a single video via animatable 3d gaussians," *arXiv preprint arXiv:2312.02134*, 2023.
- [62] S. Hu and Z. Liu, "Gauhuman: Articulated gaussian splatting from monocular human videos," *arXiv preprint arXiv:2312.02973*, 2023.
- [63] Z. Qian, S. Wang, M. Mihajlovic, A. Geiger, and S. Tang, "3dgs-avatar: Animatable avatars via deformable 3d gaussian splatting," *arXiv preprint arXiv:2312.09228*, 2023.
- [64] H. Pang, H. Zhu, A. Kortylewski, C. Theobalt, and M. Habermann, "Ash: Animatable gaussian splats for efficient and photoreal human rendering," *arXiv preprint arXiv:2312.05941*, 2023.

- [65] Z. Li, Z. Zheng, L. Wang, and Y. Liu, "Animatable gaussians: Learning pose-dependent gaussian maps for high-fidelity human avatar modeling," *arXiv preprint arXiv:2311.16096*, 2023.
- [66] M. Loper, N. Mahmood, J. Romero, G. Pons-Moll, and M. J. Black, "SMPL: A skinned multi-person linear model," *ACM Trans. Graphics (Proc. SIGGRAPH Asia)*, vol. 34, no. 6, pp. 248:1–248:16, Oct. 2015.
- [67] G. Pavlakos, V. Choutas, N. Ghorbani, T. Bolkart, A. A. A. Osman, D. Tzionas, and M. J. Black, "Expressive body capture: 3D hands, face, and body from a single image," in *Proceedings IEEE Conf. on Computer Vision and Pattern Recognition (CVPR)*, 2019, pp. 10 975–10 985.
- [68] S. Qian, T. Kirschstein, L. Schoneveld, D. Davoli, S. Giebenhain, and M. Nießner, "Gaussianavatars: Photorealistic head avatars with rigged 3d gaussians," *arXiv preprint arXiv:2312.02069*, 2023.
- [69] T. Li, T. Bolkart, M. J. Black, H. Li, and J. Romero, "Learning a model of facial shape and expression from 4D scans," *ACM Transactions on Graphics (Proc. SIGGRAPH Asia)*, vol. 36, no. 6, pp. 194:1–194:17, 2017. [Online]. Available: <https://doi.org/10.1145/3130800.3130813>
- [70] Y. Xu, B. Chen, Z. Li, H. Zhang, L. Wang, Z. Zheng, and Y. Liu, "Gaussian head avatar: Ultra high-fidelity head avatar via dynamic gaussians," *arXiv preprint arXiv:2312.03029*, 2023.
- [71] H. Luo, M. Ouyang, Z. Zhao, S. Jiang, L. Zhang, Q. Zhang, W. Yang, L. Xu, and J. Yu, "Gaussianhair: Hair modeling and rendering with light-aware gaussians," *arXiv preprint arXiv:2402.10483*, 2024.
- [72] L. Bolanos, S.-Y. Su, and H. Rhodin, "Gaussian Shadow Casting for Neural Characters," 2024.
- [73] R. Abdal, W. Yifan, Z. Shi, Y. Xu, R. Po, Z. Kuang, Q. Chen, D.-Y. Yeung, and G. Wetzstein, "Gaussian shell maps for efficient 3d human generation," *arXiv preprint arXiv:2311.17857*, 2023.
- [74] X. Liu, X. Zhan, J. Tang, Y. Shan, G. Zeng, D. Lin, X. Liu, and Z. Liu, "Humangaussian: Text-driven 3d human generation with gaussian splatting," *arXiv preprint arXiv:2311.17061*, 2023.
- [75] J. Tang, J. Ren, H. Zhou, Z. Liu, and G. Zeng, "Dreamgaussian: Generative gaussian splatting for efficient 3d content creation," *arXiv preprint arXiv:2309.16653*, 2023.
- [76] J. Ren, L. Pan, J. Tang, C. Zhang, A. Cao, G. Zeng, and Z. Liu, "Dreamgaussian4d: Generative 4d gaussian splatting," *arXiv preprint arXiv:2312.17142*, 2023.
- [77] J. Zhang, Z. Tang, Y. Pang, X. Cheng, P. Jin, Y. Wei, W. Yu, M. Ning, and L. Yuan, "Repaint123: Fast and high-quality one image to 3d generation with progressive controllable 2d repainting," *arXiv preprint arXiv:2312.13271*, 2023.
- [78] X. Zhou, X. Ran, Y. Xiong, J. He, Z. Lin, Y. Wang, D. Sun, and M.-H. Yang, "Gala3d: Towards text-to-3d complex scene generation via layout-guided generative gaussian splatting," *arXiv preprint arXiv:2402.07207*, 2024.
- [79] B. Poole, A. Jain, J. T. Barron, and B. Mildenhall, "Dreamfusion: Text-to-3d using 2d diffusion," *arXiv preprint arXiv:2209.14988*, 2022.
- [80] Z. Chen, F. Wang, and H. Liu, "Text-to-3d using gaussian splatting," *arXiv preprint arXiv:2309.16585*, 2023.
- [81] T. Yi, J. Fang, J. Wang, G. Wu, L. Xie, X. Zhang, W. Liu, Q. Tian, and X. Wang, "Gaussiandreamer: Fast generation from text to 3d gaussians by bridging 2d and 3d diffusion models," *arXiv preprint arXiv*, vol. 2310, 2023.
- [82] A. Nichol, H. Jun, P. Dhariwal, P. Mishkin, and M. Chen, "Point-e: A system for generating 3d point clouds from complex prompts," *arXiv preprint arXiv:2212.08751*, 2022.
- [83] Z. Wang, C. Lu, Y. Wang, F. Bao, C. Li, H. Su, and J. Zhu, "Prolificdreamer: High-fidelity and diverse text-to-3d generation with variational score distillation," *Advances in Neural Information Processing Systems*, vol. 36, 2024.
- [84] X. Li, H. Wang, and K.-K. Tseng, "Gaussiandiffusion: 3d gaussian splatting for denoising diffusion probabilistic models with structured noise," *arXiv preprint arXiv:2311.11221*, 2023.
- [85] Y. Liang, X. Yang, J. Lin, H. Li, X. Xu, and Y. Chen, "Luciddreamer: Towards high-fidelity text-to-3d generation via interval score matching," *arXiv preprint arXiv:2311.11284*, 2023.
- [86] J. Song, C. Meng, and S. Ermon, "Denoising diffusion implicit models," *arXiv preprint arXiv:2010.02502*, 2020.
- [87] D. Di, J. Yang, C. Luo, Z. Xue, W. Chen, X. Yang, and Y. Gao, "Hyper3dg: Text-to-3d gaussian generation via hypergraph," *arXiv preprint arXiv:2403.09236*, 2024.
- [88] Y. Feng, H. You, Z. Zhang, R. Ji, and Y. Gao, "Hypergraph neural networks," in *Proceedings of the AAAI conference on artificial intelligence*, vol. 33, no. 01, 2019, pp. 3558–3565.
- [89] X. Yang, Y. Chen, C. Chen, C. Zhang, Y. Xu, X. Yang, F. Liu, and G. Lin, "Learn to optimize denoising scores for 3d generation: A unified and improved diffusion prior on nerf and 3d gaussian splatting," *arXiv preprint arXiv:2312.04820*, 2023.
- [90] E. J. Hu, Y. Shen, P. Wallis, Z. Allen-Zhu, Y. Li, S. Wang, L. Wang, and W. Chen, "Lora: Low-rank adaptation of large language models," *arXiv preprint arXiv:2106.09685*, 2021.
- [91] L. Melas-Kyriazi, I. Laina, C. Rupprecht, N. Neverova, A. Vedaldi, O. Gafni, and F. Kokkinos, "Im-3d: Iterative multiview diffusion and reconstruction for high-quality 3d generation," *arXiv preprint arXiv:2402.08682*, 2024.
- [92] J. Tang, Z. Chen, X. Chen, T. Wang, G. Zeng, and Z. Liu, "Lgm: Large multi-view gaussian model for high-resolution 3d content creation," *arXiv preprint arXiv:2402.05054*, 2024.
- [93] L. Jiang and L. Wang, "Brightdreamer: Generic 3d gaussian generative framework for fast text-to-3d synthesis," *arXiv preprint arXiv:2403.11273*, 2024.
- [94] X. He, J. Chen, S. Peng, D. Huang, Y. Li, X. Huang, C. Yuan, W. Ouyang, and T. He, "Gvgen: Text-to-3d generation with volumetric representation," *arXiv preprint arXiv:2403.12957*, 2024.
- [95] S. D. Porumbescu, B. Budge, L. Feng, and K. I. Joy, "Shell maps," *ACM Transactions on Graphics (TOG)*, vol. 24, no. 3, pp. 626–633, 2005.
- [96] Q. Feng, Z. Xing, Z. Wu, and Y.-G. Jiang, "Fdgaussian: Fast gaussian splatting from single image via geometric-aware diffusion model," *arXiv preprint arXiv:2403.10242*, 2024.
- [97] R. Liu, R. Wu, B. Van Hoorick, P. Tokmakov, S. Zakharov, and C. Vondrick, "Zero-1-to-3: Zero-shot one image to 3d object," in *Proceedings of the IEEE/CVF International Conference on Computer Vision*, 2023, pp. 9298–9309.
- [98] A. Vilesov, P. Chari, and A. Kadambi, "Cg3d: Compositional generation for text-to-3d via gaussian splatting," *arXiv preprint arXiv:2311.17907*, 2023.
- [99] J. D. Gardiner, J. Behnsen, and C. A. Brassey, "Alpha shapes: determining 3d shape complexity across morphologically diverse structures," *BMC evolutionary biology*, vol. 18, pp. 1–16, 2018.
- [100] J. Chung, S. Lee, H. Nam, J. Lee, and K. M. Lee, "Luciddreamer: Domain-free generation of 3d gaussian splatting scenes," *arXiv preprint arXiv:2311.13384*, 2023.
- [101] A. Lugmayr, M. Danelljan, A. Romero, F. Yu, R. Timofte, and L. Van Gool, "Repaint: Inpainting using denoising diffusion probabilistic models," in *Proceedings of the IEEE/CVF conference on computer vision and pattern recognition*, 2022, pp. 11 461–11 471.
- [102] H. Ouyang, K. Heal, S. Lombardi, and T. Sun, "Text2immersion: Generative immersive scene with 3d gaussians," *arXiv preprint arXiv:2312.09242*, 2023.
- [103] H. Ling, S. W. Kim, A. Torralba, S. Fidler, and K. Kreis, "Align your gaussians: Text-to-4d with dynamic 3d gaussians and composed diffusion models," *arXiv preprint arXiv:2312.13763*, 2023.
- [104] Q. Gao, Q. Xu, Z. Cao, B. Mildenhall, W. Ma, L. Chen, D. Tang, and U. Neumann, "Gaussianflow: Splatting gaussian dynamics for 4d content creation," *arXiv preprint arXiv:2403.12365*, 2024.
- [105] Y. Shi, P. Wang, J. Ye, M. Long, K. Li, and X. Yang, "Mv-dream: Multi-view diffusion for 3d generation," *arXiv preprint arXiv:2308.16512*, 2023.
- [106] Z. Guo, W. Zhou, L. Li, M. Wang, and H. Li, "Motion-aware 3d gaussian splatting for efficient dynamic scene reconstruction," *arXiv preprint arXiv:2403.11447*, 2024.
- [107] Y. Yin, D. Xu, Z. Wang, Y. Zhao, and Y. Wei, "4dgen: Grounded 4d content generation with spatial-temporal consistency," *arXiv preprint arXiv:2312.17225*, 2023.
- [108] A. Cao and J. Johnson, "Hexplane: A fast representation for dynamic scenes," in *Proceedings of the IEEE/CVF Conference on Computer Vision and Pattern Recognition*, 2023, pp. 130–141.
- [109] Z. Pan, Z. Yang, X. Zhu, and L. Zhang, "Fast dynamic 3d object generation from a single-view video," *arXiv preprint arXiv:2401.08742*, 2024.
- [110] Z. Yang, H. Yang, Z. Pan, X. Zhu, and L. Zhang, "Real-time photorealistic dynamic scene representation and rendering with 4d gaussian splatting," *arXiv preprint arXiv:2310.10642*, 2023.
- [111] T. Zhang, Q. Gao, W. Li, L. Liu, and B. Chen, "Bags: Building animatable gaussian splatting from a monocular video with diffusion priors," *arXiv preprint arXiv:2403.11427*, 2024.

- [112] X. Zhou, Z. Lin, X. Shan, Y. Wang, D. Sun, and M.-H. Yang, "Drivinggaussian: Composite gaussian splatting for surrounding dynamic autonomous driving scenes," *arXiv preprint arXiv:2312.07920*, 2023.
- [113] Y. Yan, H. Lin, C. Zhou, W. Wang, H. Sun, K. Zhan, X. Lang, X. Zhou, and S. Peng, "Street gaussians for modeling dynamic urban scenes," *arXiv preprint arXiv:2401.01339*, 2024.
- [114] H. Zhou, J. Shao, L. Xu, D. Bai, W. Qiu, B. Liu, Y. Wang, A. Geiger, and Y. Liao, "Hugs: Holistic urban 3d scene understanding via gaussian splatting," *arXiv preprint arXiv:2403.12722*, 2024.
- [115] K. Katsumata, D. M. Vo, and H. Nakayama, "An efficient 3d gaussian representation for monocular/multi-view dynamic scenes," *arXiv preprint arXiv:2311.12897*, 2023.
- [116] Q. Herau, M. Bennehar, A. Moreau, N. Piasco, L. Roldao, D. Tsishkou, C. Migniot, P. Vasseur, and C. Démonceaux, "3dgs-calib: 3d gaussian splatting for multimodal spatiotemporal calibration," *arXiv preprint arXiv:2403.11577*, 2024.
- [117] F. Tosi, Y. Zhang, Z. Gong, E. Sandström, S. Mattocchia, M. R. Oswald, and M. Poggi, "How nerfs and 3d gaussian splatting are reshaping slam: a survey," *arXiv preprint arXiv:2402.13255*, 2024.
- [118] C. Yan, D. Qu, D. Wang, D. Xu, Z. Wang, B. Zhao, and X. Li, "Gs-slam: Dense visual slam with 3d gaussian splatting," *arXiv preprint arXiv:2311.11700*, 2023.
- [119] H. Huang, L. Li, H. Cheng, and S.-K. Yeung, "Photo-slam: Real-time simultaneous localization and photorealistic mapping for monocular, stereo, and rgb-d cameras," *arXiv preprint arXiv:2311.16728*, 2023.
- [120] N. Keetha, J. Karhade, K. M. Jatavallabhula, G. Yang, S. Scherer, D. Ramanan, and J. Luiten, "Splatam: Splat, track & map 3d gaussians for dense rgb-d slam," *arXiv preprint arXiv:2312.02126*, 2023.
- [121] V. Yugay, Y. Li, T. Gevers, and M. R. Oswald, "Gaussian-slam: Photo-realistic dense slam with gaussian splatting," *arXiv preprint arXiv:2312.10070*, 2023.
- [122] M. Li, S. Liu, and H. Zhou, "Sgs-slam: Semantic gaussian splatting for neural dense slam," *arXiv preprint arXiv:2402.03246*, 2024.
- [123] E. Rublee, V. Rabaud, K. Konolige, and G. Bradski, "Orb: An efficient alternative to sift or surf," in *2011 International conference on computer vision*. Ieee, 2011, pp. 2564–2571.
- [124] J. J. Moré, "The levenberg-marquardt algorithm: implementation and theory," in *Numerical analysis: proceedings of the biennial Conference held at Dundee, June 28–July 1, 1977*. Springer, 2006, pp. 105–116.
- [125] Z. Teed and J. Deng, "Droid-slam: Deep visual slam for monocular, stereo, and rgb-d cameras," *Advances in neural information processing systems*, vol. 34, pp. 16 558–16 569, 2021.
- [126] H. Matsuki, R. Murai, P. H. Kelly, and A. J. Davison, "Gaussian splatting slam," *arXiv preprint arXiv:2312.06741*, 2023.
- [127] S. Ha, J. Yeon, and H. Yu, "Rgb-d gs-icp slam," *arXiv preprint arXiv:2403.12550*, 2024.
- [128] A. Segal, D. Haehnel, and S. Thrun, "Generalized-icp." in *Robotics: science and systems*, vol. 2, no. 4. Seattle, WA, 2009, p. 435.
- [129] S. Sun, M. Mielle, A. J. Lilienthal, and M. Magnusson, "High-fidelity slam using gaussian splatting with rendering-guided densification and regularized optimization," *arXiv preprint arXiv:2403.12535*, 2024.
- [130] S. Zhu, R. Qin, G. Wang, J. Liu, and H. Wang, "Semgauss-slam: Dense semantic gaussian splatting slam," *arXiv preprint arXiv:2403.07494*, 2024.
- [131] Y. Ji, Y. Liu, G. Xie, B. Ma, and Z. Xie, "Neds-slam: A novel neural explicit dense semantic slam framework using 3d gaussian splatting," *arXiv preprint arXiv:2403.11679*, 2024.
- [132] L. Yang, B. Kang, Z. Huang, X. Xu, J. Feng, and H. Zhao, "Depth anything: Unleashing the power of large-scale unlabeled data," *arXiv preprint arXiv:2401.10891*, 2024.
- [133] P. Jiang, G. Pandey, and S. Saripalli, "3dgs-reloc: 3d gaussian splatting for map representation and visual relocalization," *arXiv preprint arXiv:2403.11367*, 2024.
- [134] X. Lei, M. Wang, W. Zhou, and H. Li, "Gaussnav: Gaussian splatting for visual navigation," *arXiv preprint arXiv:2403.11625*, 2024.
- [135] J. Luiten, G. Kopanas, B. Leibe, and D. Ramanan, "Dynamic 3d gaussians: Tracking by persistent dynamic view synthesis," *arXiv preprint arXiv:2308.09713*, 2023.
- [136] Y. Wang, X. Yi, Z. Wu, N. Zhao, L. Chen, and H. Zhang, "View-consistent 3d editing with gaussian splatting," *arXiv preprint arXiv:2403.11868*, 2024.
- [137] B. Huang, Z. Yu, A. Chen, A. Geiger, and S. Gao, "2d gaussian splatting for geometrically accurate radiance fields," *arXiv preprint arXiv:2403.17888*, 2024.
- [138] J.-C. Shi, M. Wang, H.-B. Duan, and S.-H. Guan, "Language embedded 3d gaussians for open-vocabulary scene understanding," *arXiv preprint arXiv:2311.18482*, 2023.
- [139] T. Xie, Z. Zong, Y. Qiu, X. Li, Y. Feng, Y. Yang, and C. Jiang, "Physgaussian: Physics-integrated 3d gaussians for generative dynamics," *arXiv preprint arXiv:2311.12198*, 2023.
- [140] J. Sun, H. Jiao, G. Li, Z. Zhang, L. Zhao, and W. Xing, "3dgs-stream: On-the-fly training of 3d gaussians for efficient streaming of photo-realistic free-viewpoint videos," *arXiv preprint arXiv:2403.01444*, 2024.
- [141] R. Shaw, J. Song, A. Moreau, M. Nazarczuk, S. Catley-Chandar, H. Dharmo, and E. Perez-Pellitero, "Swags: Sampling windows adaptively for dynamic 3d gaussian splatting," *arXiv preprint arXiv:2312.13308*, 2023.
- [142] Y. Xiao, X. Wang, J. Li, H. Cai, Y. Fan, N. Xue, M. Yang, Y. Shen, and S. Gao, "Bridging 3d gaussian and mesh for freeview video rendering," *arXiv preprint arXiv:2403.11453*, 2024.
- [143] Z. Yang, X. Gao, W. Zhou, S. Jiao, Y. Zhang, and X. Jin, "Deformable 3d gaussians for high-fidelity monocular dynamic scene reconstruction," *arXiv preprint arXiv:2309.13101*, 2023.
- [144] Y. Liang, N. Khan, Z. Li, T. Nguyen-Phuoc, D. Lanman, J. Tompkin, and L. Xiao, "Gaufre: Gaussian deformation fields for real-time dynamic novel view synthesis," *arXiv preprint arXiv:2312.11458*, 2023.
- [145] G. Wu, T. Yi, J. Fang, L. Xie, X. Zhang, W. Wei, W. Liu, Q. Tian, and X. Wang, "4d gaussian splatting for real-time dynamic scene rendering," *arXiv preprint arXiv:2310.08528*, 2023.
- [146] B. P. Duijsterhof, Z. Mandi, Y. Yao, J.-W. Liu, M. Z. Shou, S. Song, and J. Ichnowski, "Md-splatting: Learning metric deformation from 4d gaussians in highly deformable scenes," *arXiv preprint arXiv:2312.00583*, 2023.
- [147] A. Kratimenos, J. Lei, and K. Daniilidis, "Dynmf: Neural motion factorization for real-time dynamic view synthesis with 3d gaussian splatting," *arXiv preprint arXiv:2312.00112*, 2023.
- [148] Z. Li, Z. Chen, Z. Li, and Y. Xu, "Spacetime gaussian feature splatting for real-time dynamic view synthesis," *arXiv preprint arXiv:2312.16812*, 2023.
- [149] Y. Lin, Z. Dai, S. Zhu, and Y. Yao, "Gaussian-flow: 4d reconstruction with dynamic 3d gaussian particle," *arXiv preprint arXiv:2312.03431*, 2023.
- [150] Y.-H. Huang, Y.-T. Sun, Z. Yang, X. Lyu, Y.-P. Cao, and X. Qi, "Sc-gs: Sparse-controlled gaussian splatting for editable dynamic scenes," *arXiv preprint arXiv:2312.14937*, 2023.
- [151] R. W. Sumner, J. Schmid, and M. Pauly, "Embedded deformation for shape manipulation," in *ACM siggraph 2007 papers*, 2007, pp. 80–es.
- [152] Y. Duan, F. Wei, Q. Dai, Y. He, W. Chen, and B. Chen, "4d gaussian splatting: Towards efficient novel view synthesis for dynamic scenes," *arXiv preprint arXiv:2402.03307*, 2024.
- [153] H. Chen, C. Li, and G. H. Lee, "Neusg: Neural implicit surface reconstruction with 3d gaussian splatting guidance," *arXiv preprint arXiv:2312.00846*, 2023.
- [154] P. Wang, L. Liu, Y. Liu, C. Theobalt, T. Komura, and W. Wang, "Neus: Learning neural implicit surfaces by volume rendering for multi-view reconstruction," *arXiv preprint arXiv:2106.10689*, 2021.
- [155] A. Gropp, L. Yariv, N. Haim, M. Atzmon, and Y. Lipman, "Implicit geometric regularization for learning shapes," *arXiv preprint arXiv:2002.10099*, 2020.
- [156] A. Guédon and V. Lepetit, "Sugar: Surface-aligned gaussian splatting for efficient 3d mesh reconstruction and high-quality mesh rendering," *arXiv preprint arXiv:2311.12775*, 2023.
- [157] W. E. Lorensen and H. E. Cline, "Marching cubes: A high resolution 3d surface construction algorithm," in *Seminal graphics: pioneering efforts that shaped the field*, 1998, pp. 347–353.
- [158] X. Lyu, Y.-T. Sun, Y.-H. Huang, X. Wu, Z. Yang, Y. Chen, J. Pang, and X. Qi, "3dgsr: Implicit surface reconstruction with 3d gaussian splatting," *arXiv preprint arXiv:2404.00409*, 2024.
- [159] M. Yu, T. Lu, L. Xu, L. Jiang, Y. Xiangli, and B. Dai, "Gsd: 3dgs meets sdf for improved rendering and reconstruction," *arXiv preprint arXiv:2403.16964*, 2024.
- [160] P. Dai, J. Xu, W. Xie, X. Liu, H. Wang, and W. Xu, "High-quality surface reconstruction using gaussian surfels," *arXiv preprint arXiv:2404.17774*, 2024.

- [161] Z. Yu, T. Sattler, and A. Geiger, "Gaussian opacity fields: Efficient and compact surface reconstruction in unbounded scenes," *arXiv preprint arXiv:2404.10772*, 2024.
- [162] Y. Chen, Z. Chen, C. Zhang, F. Wang, X. Yang, Y. Wang, Z. Cai, L. Yang, H. Liu, and G. Lin, "Gaussianeditor: Swift and controllable 3d editing with gaussian splatting," *arXiv preprint arXiv:2311.14521*, 2023.
- [163] F. Palandra, A. Sanchietti, D. Baieri, and E. Rodolà, "Gsedite: Efficient text-guided editing of 3d objects via gaussian splatting," *arXiv preprint arXiv:2403.05154*, 2024.
- [164] T. Brooks, A. Holynski, and A. A. Efros, "Instructpix2pix: Learning to follow image editing instructions," in *Proceedings of the IEEE/CVF Conference on Computer Vision and Pattern Recognition, 2023*, pp. 18392–18402.
- [165] J. Fang, J. Wang, X. Zhang, L. Xie, and Q. Tian, "Gaussianeditor: Editing 3d gaussians delicately with text instructions," *arXiv preprint arXiv:2311.16037*, 2023.
- [166] J. Wu, J.-W. Bian, X. Li, G. Wang, I. Reid, P. Torr, and V. A. Prisacariu, "Gausctrl: Multi-view consistent text-driven 3d gaussian splatting editing," *arXiv preprint arXiv:2403.08733*, 2024.
- [167] L. Zhang, A. Rao, and M. Agrawala, "Adding conditional control to text-to-image diffusion models," in *Proceedings of the IEEE/CVF International Conference on Computer Vision, 2023*, pp. 3836–3847.
- [168] R. Shao, J. Sun, C. Peng, Z. Zheng, B. Zhou, H. Zhang, and Y. Liu, "Control4d: Dynamic portrait editing by learning 4d gan from 2d diffusion-based editor," *arXiv preprint arXiv:2305.20082*, vol. 2, no. 6, p. 16, 2023.
- [169] I. Goodfellow, J. Pouget-Abadie, M. Mirza, B. Xu, D. Warde-Farley, S. Ozair, A. Courville, and Y. Bengio, "Generative adversarial networks," *Communications of the ACM*, vol. 63, no. 11, pp. 139–144, 2020.
- [170] J. Zhuang, D. Kang, Y.-P. Cao, G. Li, L. Lin, and Y. Shan, "Tip-editor: An accurate 3d editor following both text-prompts and image-prompts," *arXiv preprint arXiv:2401.14828*, 2024.
- [171] J. Huang and H. Yu, "Point'n move: Interactive scene object manipulation on gaussian splatting radiance fields," *arXiv preprint arXiv:2311.16737*, 2023.
- [172] A. Saroha, M. Gladkova, C. Curreli, T. Yenamandra, and D. Cremers, "Gaussian splatting in style," *arXiv preprint arXiv:2403.08498*, 2024.
- [173] Y.-H. Huang, Y. He, Y.-J. Yuan, Y.-K. Lai, and L. Gao, "Stylizednerf: consistent 3d scene stylization as stylized nerf via 2d-3d mutual learning," in *Proceedings of the IEEE/CVF Conference on Computer Vision and Pattern Recognition, 2022*, pp. 18342–18352.
- [174] H. Yu, J. Julin, Z. Á. Milacski, K. Niinuma, and L. A. Jeni, "Cogs: Controllable gaussian splatting," *arXiv preprint arXiv:2312.05664*, 2023.
- [175] S. Zhou, H. Chang, S. Jiang, Z. Fan, Z. Zhu, D. Xu, P. Chari, S. You, Z. Wang, and A. Kadambi, "Feature 3dgs: Supercharging 3d gaussian splatting to enable distilled feature fields," *arXiv preprint arXiv:2312.03203*, 2023.
- [176] M. Ye, M. Danelljan, F. Yu, and L. Ke, "Gaussian grouping: Segment and edit anything in 3d scenes," *arXiv preprint arXiv:2312.00732*, 2023.
- [177] H. K. Cheng, S. W. Oh, B. Price, A. Schwing, and J.-Y. Lee, "Tracking anything with decoupled video segmentation," in *Proceedings of the IEEE/CVF International Conference on Computer Vision, 2023*, pp. 1316–1326.
- [178] A. Kirillov, E. Mintun, N. Ravi, H. Mao, C. Rolland, L. Gustafson, T. Xiao, S. Whitehead, A. C. Berg, W.-Y. Lo *et al.*, "Segment anything," in *Proceedings of the IEEE/CVF International Conference on Computer Vision, 2023*, pp. 4015–4026.
- [179] K. Lan, H. Li, H. Shi, W. Wu, Y. Liao, L. Wang, and P. Zhou, "2d-guided 3d gaussian segmentation," *arXiv preprint arXiv:2312.16047*, 2023.
- [180] B. Dou, T. Zhang, Y. Ma, Z. Wang, and Z. Yuan, "Cosseggaussians: Compact and swift scene segmenting 3d gaussians," *arXiv preprint arXiv:2401.05925*, 2024.
- [181] M. Qin, W. Li, J. Zhou, H. Wang, and H. Pfister, "Langsplat: 3d language gaussian splatting," *arXiv preprint arXiv:2312.16084*, 2023.
- [182] X. Zuo, P. Samangouei, Y. Zhou, Y. Di, and M. Li, "Fmgs: Foundation model embedded 3d gaussian splatting for holistic 3d scene understanding," *arXiv preprint arXiv:2401.01970*, 2024.
- [183] A. Radford, J. W. Kim, C. Hallacy, A. Ramesh, G. Goh, S. Agarwal, G. Sastry, A. Askell, P. Mishkin, J. Clark *et al.*, "Learning transferable visual models from natural language supervision," in *International conference on machine learning*. PMLR, 2021, pp. 8748–8763.
- [184] M. Caron, H. Touvron, I. Misra, H. Jégou, J. Mairal, P. Bojanowski, and A. Joulin, "Emerging properties in self-supervised vision transformers," in *Proceedings of the IEEE/CVF international conference on computer vision, 2021*, pp. 9650–9660.
- [185] A. Van Den Oord, O. Vinyals *et al.*, "Neural discrete representation learning," *Advances in neural information processing systems*, vol. 30, 2017.
- [186] A. De Vaucorbeil, V. P. Nguyen, S. Sinaie, and J. Y. Wu, "Material point method after 25 years: theory, implementation, and applications," *Advances in applied mechanics*, vol. 53, pp. 185–398, 2020.
- [187] J. Jung, J. Han, H. An, J. Kang, S. Park, and S. Kim, "Relaxing accurate initialization constraint for 3d gaussian splatting," *arXiv preprint arXiv:2403.09413*, 2024.
- [188] D. Das, C. Wewer, R. Yunus, E. Ilg, and J. E. Lenssen, "Neural parametric gaussians for monocular non-rigid object reconstruction," *arXiv preprint arXiv:2312.01196*, 2023.
- [189] J. Lei, Y. Wang, G. Pavlakos, L. Liu, and K. Daniilidis, "Gart: Gaussian articulated template models," *arXiv preprint arXiv:2311.16099*, 2023.
- [190] L. Huang, J. Bai, J. Guo, and Y. Guo, "Gs++: Error analyzing and optimal gaussian splatting," *arXiv preprint arXiv:2402.00752*, 2024.
- [191] L. Franke, D. Rückert, L. Fink, and M. Stamminger, "Trips: Trilinear point splatting for real-time radiance field rendering," in *Computer Graphics Forum*. Wiley Online Library, 2024, p. e15012.
- [192] Y. Li, C. Lyu, Y. Di, G. Zhai, G. H. Lee, and F. Tombari, "Geogaussian: Geometry-aware gaussian splatting for scene rendering," *arXiv preprint arXiv:2403.11324*, 2024.
- [193] H. Xiong, S. Muttukuru, R. Upadhyay, P. Chari, and A. Kadambi, "Sparsesegs: Real-time 360  $\{\deg\}$  sparse view synthesis using gaussian splatting," *arXiv preprint arXiv:2312.00206*, 2023.
- [194] L. Bolanos, S.-Y. Su, and H. Rhodin, "Gaussian shadow casting for neural characters," in *Proceedings of the IEEE/CVF Conference on Computer Vision and Pattern Recognition, 2024*, pp. 20997–21006.
- [195] Y. Liu, C. Lin, Z. Zeng, X. Long, L. Liu, T. Komura, and W. Wang, "Syncdreamer: Generating multiview-consistent images from a single-view image," *arXiv preprint arXiv:2309.03453*, 2023.
- [196] Z. Li, Y. Chen, L. Zhao, and P. Liu, "Controllable text-to-3d generation via surface-aligned gaussian splatting," *arXiv preprint arXiv:2403.09981*, 2024.
- [197] M. Armandpour, A. Sadeghian, H. Zheng, A. Sadeghian, and M. Zhou, "Re-imagine the negative prompt algorithm: Transform 2d diffusion into 3d, alleviate janus problem and beyond," *arXiv preprint arXiv:2304.04968*, 2023.
- [198] Z. Zhang, W. Hu, Y. Lao, T. He, and H. Zhao, "Pixel-gs: Density control with pixel-aware gradient for 3d gaussian splatting," *arXiv preprint arXiv:2403.15530*, 2024.
- [199] Q. Feng, G. Cao, H. Chen, T.-J. Mu, R. R. Martin, and S.-M. Hu, "A new split algorithm for 3d gaussian splatting," *arXiv preprint arXiv:2403.09143*, 2024.
- [200] M. Niemeyer, F. Manhardt, M.-J. Rakotosaona, M. Oechsle, D. Duckworth, R. Gosula, K. Tateno, J. Bates, D. Kaeser, and F. Tombari, "Radsplat: Radiance field-informed gaussian splatting for robust real-time rendering with 900+ fps," *arXiv preprint arXiv:2403.13806*, 2024.
- [201] G. Fang and B. Wang, "Mini-splatting: Representing scenes with a constrained number of gaussians," *arXiv preprint arXiv:2403.14166*, 2024.
- [202] M. Kazhdan, M. Bolitho, and H. Hoppe, "Poisson surface reconstruction," in *Proceedings of the fourth Eurographics symposium on Geometry processing*, vol. 7, no. 4, 2006.
- [203] J. Tang, H. Zhou, X. Chen, T. Hu, E. Ding, J. Wang, and G. Zeng, "Delicate textured mesh recovery from nerf via adaptive surface refinement," in *Proceedings of the IEEE/CVF International Conference on Computer Vision, 2023*, pp. 17739–17749.
- [204] H. Li, Y. Gao, D. Zhang, C. Wu, Y. Dai, C. Zhao, H. Feng, E. Ding, J. Wang, and J. Han, "Ggrt: Towards generalizable 3d gaussians without pose priors in real-time," *arXiv preprint arXiv:2403.10147*, 2024.
- [205] D. Malarz, W. Smolak, J. Tabor, S. Tadeja, and P. Spurek, "Gaussian splatting with nerf-based color and opacity."
- [206] S. Zuffi, A. Kanazawa, D. W. Jacobs, and M. J. Black, "3d menagerie: Modeling the 3d shape and pose of animals," in *Proceedings of the IEEE conference on computer vision and pattern recognition, 2017*, pp. 6365–6373.

- [207] Z. Fan, W. Cong, K. Wen, K. Wang, J. Zhang, X. Ding, D. Xu, B. Ivanovic, M. Pavone, G. Pavlakos *et al.*, “Instantsplat: Unbounded sparse-view pose-free gaussian splatting in 40 seconds,” *arXiv preprint arXiv:2403.20309*, 2024.
- [208] Y. Sun, X. Wang, Y. Zhang, J. Zhang, C. Jiang, Y. Guo, and F. Wang, “icomma: Inverting 3d gaussians splatting for camera pose estimation via comparing and matching,” *arXiv preprint arXiv:2312.09031*, 2023.
- [209] R. Martin-Brualla, N. Radwan, M. S. Sajjadi, J. T. Barron, A. Dosovitskiy, and D. Duckworth, “Nerf in the wild: Neural radiance fields for unconstrained photo collections,” in *Proceedings of the IEEE/CVF conference on computer vision and pattern recognition*, 2021, pp. 7210–7219.
- [210] X. Chen, Q. Zhang, X. Li, Y. Chen, Y. Feng, X. Wang, and J. Wang, “Hallucinated neural radiance fields in the wild,” in *Proceedings of the IEEE/CVF Conference on Computer Vision and Pattern Recognition*, 2022, pp. 12 943–12 952.
- [211] Y. Yang, S. Zhang, Z. Huang, Y. Zhang, and M. Tan, “Cross-ray neural radiance fields for novel-view synthesis from unconstrained image collections,” in *Proceedings of the IEEE/CVF International Conference on Computer Vision*, 2023, pp. 15 901–15 911.
- [212] H. Dahmani, M. Bennehar, N. Piasco, L. Roldao, and D. Tsishkou, “Swag: Splatting in the wild images with appearance-conditioned gaussians,” *arXiv preprint arXiv:2403.10427*, 2024.
- [213] D. Zhang, C. Wang, W. Wang, P. Li, M. Qin, and H. Wang, “Gaussian in the wild: 3d gaussian splatting for unconstrained image collections,” *arXiv preprint arXiv:2403.15704*, 2024.
- [214] Y. Fu, S. Liu, A. Kulkarni, J. Kautz, A. A. Efros, and X. Wang, “Colmap-free 3d gaussian splatting,” *arXiv preprint arXiv:2312.07504*, 2023.
- [215] D. Cai, J. Heikkilä, and E. Rahtu, “Gs-pose: Cascaded framework for generalizable segmentation-based 6d object pose estimation,” *arXiv preprint arXiv:2403.10683*, 2024.
- [216] Z. Liang, Q. Zhang, Y. Feng, Y. Shan, and K. Jia, “Gs-ir: 3d gaussian splatting for inverse rendering,” in *Proceedings of the IEEE/CVF Conference on Computer Vision and Pattern Recognition*, 2024, pp. 21 644–21 653.
- [217] S. Saito, G. Schwartz, T. Simon, J. Li, and G. Nam, “Relightable gaussian codec avatars,” in *Proceedings of the IEEE/CVF Conference on Computer Vision and Pattern Recognition*, 2024, pp. 130–141.
- [218] J. Lin, Z. Li, X. Tang, J. Liu, S. Liu, J. Liu, Y. Lu, X. Wu, S. Xu, Y. Yan *et al.*, “Vastgaussian: Vast 3d gaussians for large scene reconstruction,” *arXiv preprint arXiv:2402.17427*, 2024.
- [219] T. Suzuki, “Fed3dgs: Scalable 3d gaussian splatting with federated learning,” *arXiv preprint arXiv:2403.11460*, 2024.
- [220] L. Zhu, Z. Wang, J. Cui, Z. Jin, G. Lin, and L. Yu, “Endogs: Deformable endoscopic tissues reconstruction with gaussian splatting.”
- [221] M. Kruse, M. Rudolph, D. Woiwode, and B. Rosenhahn, “Splatpose & detect: Pose-agnostic 3d anomaly detection,” in *Proceedings of the IEEE/CVF Conference on Computer Vision and Pattern Recognition*, 2024, pp. 3950–3960.
- [222] X. Zhang, X. Ge, T. Xu, D. He, Y. Wang, H. Qin, G. Lu, J. Geng, and J. Zhang, “Gaussianimage: 1000 fps image representation and compression by 2d gaussian splatting,” *arXiv preprint arXiv:2403.08551*, 2024.
- [223] V. M. Nguyen, E. Sandidge, T. Mahendrakar, and R. T. White, “Characterizing satellite geometry via accelerated 3d gaussian splatting,” *Aerospace*, vol. 11, no. 3, p. 183, 2024.
- [224] G. Wang, L. Pan, S. Peng, S. Liu, C. Xu, Y. Miao, W. Zhan, M. Tomizuka, M. Pollefeys, and H. Wang, “Nerf in robotics: A survey,” *arXiv preprint arXiv:2405.01333*, 2024.
- [225] E. Alcaide, S. Biderman, A. Telenti, and M. C. Maher, “Mp-nerf: A massively parallel method for accelerating protein structure reconstruction from internal coordinates,” *Journal of Computational Chemistry*, vol. 43, no. 1, pp. 74–78, 2022.